Accepted Manuscript

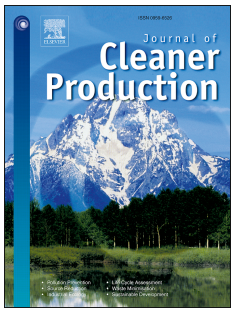

Organic Rankine Cycle system performance targeting and design for multiple heat sources with simultaneous working fluid selection

Mirko Z. Stijepovic, Athanasios I. Papadopoulos, Patrick Linke, Vladimir Stijepovic, Aleksandar S. Grujic, Mirjana Kijevčanin, Panos Seferlis

PII: S0959-6526(16)31933-3

DOI: 10.1016/j.jclepro.2016.11.088

Reference: JCLP 8477

To appear in: *Journal of Cleaner Production*

Received Date: 8 August 2016

Revised Date: 6 October 2016

Accepted Date: 15 November 2016

Please cite this article as: Stijepovic MZ, Papadopoulos AI, Linke P, Stijepovic V, Grujic AS, Kijevčanin M, Seferlis P, Organic Rankine Cycle system performance targeting and design for multiple heat sources with simultaneous working fluid selection, *Journal of Cleaner Production* (2016), doi: 10.1016/j.jclepro.2016.11.088.

Organic Rankine Cycle System Performance Targeting and Design for Multiple Heat Sources with Simultaneous Working Fluid Selection

Mirko Z. Stijepovic[a,b,d], Athanasios I. Papadopoulos[c], Patrick Linke[b], Vladimir Stijepovic[a], Aleksandar S. Grujic[d], Mirjana Kijevčanin[a], Panos Seferlis[e]

[a] Faculty of Technology and Metallurgy, University of Belgrade, Karnegijeva 4, 11000 Belgrade, Serbia

[b] Department of Chemical Engineering, Texas A&M University at Qatar, PO Box 23874, Education City, Doha, Qatar

[c]Chemical and Process Engineering Research Institute, Centre for Research and Technology-Hellas, Thermi 57001, Thessaloniki, Greece

[d] Institute of Chemistry, Technology and Metallurgy, University of Belgrade, Njegoševa 12, 11000 Belgrade, Serbia

[e]Department of Mechanical Engineering, Aristotle University of Thessaloniki, P.O. Box 484, 54124 Thessaloniki, Greece

ABSTRACT

This work presents a systematic approach toward the design of Organic Rankine Cycles (ORC) for the generation of power from multiple heat sources available at different temperature levels. The design problem is approached in a mixed-integer non-linear programming (MINLP) formulation where an inclusive and flexible ORC model is automatically evolved by a

deterministic algorithm for global optimization. The basic building block of the model is the ORC cascade which consists of a heat extraction, a power generation, a condensation and a liquid pressurization section. The aim of the optimization is to determine the optimum number of ORC cascades, the structure of the heat exchanger network shared among different cascades, the operating conditions and the working fluid used in each cascade in order to identify an overall ORC structure that maximizes the power output. The approach is illustrated through a case study which indicates that a system of two waste heat sources is best exploited through two interconnected ORC utilizing different working fluids.

Keywords: Organic Rankine Cycle, optimization, working fluids, multiple heat sources, pinch analysis

1. Introduction

In order to protect the environment and support sustainable development, clean and efficient substitutes to existing power production systems primarily driven by combustion of fossil fuels are needed. In the last decade, extensive research has been conducted to develop novel power generation systems capable of converting thermal energy to power from diverse renewable sources and waste heat in a more efficient and sustainable manner than the conventional systems. Potential renewable energy sources are: biofuels, biomass, municipal waste, solar, geothermal, wind, and ocean heat. Large quantities of energy in industrial plants are lost via exhaust gases liquid streams and cooling water. Low grade energy share is the largest in the waste heat pool. Currently, the share of waste heat recovery contribution to the total energy usage is still negligible. Liu et al. presented study in which Organic Rankine Cycles (ORC) is employed to generate power from low grade heat produced in compressor stage of carbon capture process [1]. Uusitalo et al. used ORC to recover low grade heat from exhaust gas from bio-engine [2]. Conor Walsh and Patricia Thornley presented paper in which ORC is used to generate power from stack of coke oven used in steel plant [3]. The European Union estimates a theoretical potential of about 2.5 GW of gross electric power which could be produced from available waste heat by Organic Rankine Cycles (ORC) [4].

The ORC has been broadly studied and employed to generate or co-generate power from low to moderate temperature heat sources. It employs organic working fluids to generate mechanical work and power more efficiently than conventional water-based cycles for heat sources in the temperature range from 80°C to 400°C [5]. ORC have significant advantages over other technologies due to the simplicity in the cycle configuration, low maintenance requirements, ability to perform under part load conditions and to adapt to different heat source temperature

profiles [6]. The reference ORC technology is a subcritical Organic Rankine Cycle (SORC). The SORC is consisted of heat extraction, power production, condensation and liquid pressurization sections, with the working fluid operating at subcritical conditions. One of the main challenges to attain high performance SORC is the reduction of the irreversibilities during energy conversion in key processes. Pinch point limitations in the evaporator and condenser increase irreversibility due to finite heat transfer. This is more pronounced when pure working fluids are used because flat boiling temperature profile leads to poor thermal match during the heat transfer. Exit losses in the cycle may be decreased by reducing pinch point limitations. This could be accomplished by employing suitable pure or mixed working fluid, as well as proper SORC integration with the neighboring processes.

A large number of published works is devoted to the problem of selecting suitable working fluids and operating conditions for a particular heat source using various criteria [7-16]. The insights obtained from these studies stress the importance of selecting working fluids with suitable properties to achieve optimal ORC performance. The role of working fluid properties on the ORC performance is considered by Stijepovic et al. [17]. An inclusive summary of approaches regarding the evaluation of ORC process performance and selection of working fluid is provided in review article reported by Bao and Zhao [18].

The ORC operating and economic performance also depends on the type of equipment as well as the way that different equipment components are interconnected and integrated with the surrounding processes. Several published works consider different ORC configurations to help improve the performance of a SORC process. Some authors [7,19] propose the addition of a recuperator in SORC to reuse the heat after the turbine in order to preheat the working fluid. A recuperator increases thermal efficiency and can be beneficial for waste heat recovery

applications, in cases when there is a bound on heat carrier outlet temperature [20]. Mago et al. [21] presented an analysis of regenerative ORC. The obtained results indicate that they have a higher thermal efficiency and lower irrevesibilities than conventional SORC. The organic flash cycle (OFC) is another type of configuration where the organic fluid is heated to its boiling point. This is done by ensuring that boiling is avoided at the heat exchanger to enable a better match between the temperature profiles of the heat carrier. After heating, the working fluid is throttled down to a lower pressure in a flash vessel. Vapor is directed to the turbine inlet while the liquid is mixed with the turbine exit and directed to the condenser [20]. These cycles have lower thermal efficiency then SORC, but they have better heat recovery and higher power output [20]. The trilateral cycle is similar to OFC but instead of flashing the working fluid to produce saturated vapor and saturated liquid it is directly fed to the turbine. The trilateral cycle has a lower thermal efficiency than SORC [22]. However, there is a higher potential to recover heat because of the better match between the temperature profiles of the heat carrier and working fluid. Moreover, to improve SORC performance the employment of transcritical cycles (TC) is also an option. The TC has the same layout as SORC but the liquid to vapor phase transition is performed at supercritical pressure. Schuster et al. [23] state that the TC has lower thermal efficiency than SORC, but generates higher power output. Vapor reheating has also been considered as a method to increase the thermal efficiency. Different pressure levels can be exploited in a primary high pressure turbine and a subsequent low pressure turbine where the reheated vapor produces additional work as it expands to the condenser pressure [21]. This type of cycle increases thermal efficiency and power output. Another modification of SORC includes multiple evaporation pressure loops providing good match between the high temperature side of the heat carrier and the high pressure loop, enabling high thermal efficiency [24]. An inclusive

summary of approaches regarding the evaluation of ORC architecture for waste heat recovery is provided in a review article reported by Lecompte et al. [20].

Although such configurations are beneficial, efficient integration with the underlying heat source is essential in order to exploit such benefits. In industrial environments the integration of SORCs needs to account for multiple heat sources with different temperature and flow characteristics. This is a challenging problem which requires the use of systematic process integration methods [25]. Although such methods are based on the graphical Pinch analysis approach [26], the underlying principles may also be transformed into mathematical models to support process simulation or optimization. Several graphical or simulation based approaches have been reported for integrating ORC with the background heat sources [5,27-31]. Desai and Bandyopadhyay [27] observe that by using Pinch analysis (e.g. grand composite curves) it is possible to analyze complex heat exchange configurations. Furthermore, it is also possible to decide how to place ORC equipment within the background (heat source) process in order to maximize the overall performance. The resulting improvements are based on an ORC configuration involving turbine bleeding with regeneration. Song et al. [31] explore integration schemes for single and dual ORCs with multiple waste heat streams through simulation. The work identifies the dual cycle as the best performing configuration for a refinery case study. This highlights the need to develop optimal ORC integration methods in the future that can take into account multiple heat source streams and multiple integrated power cycles simultaneously. DiGenova et al. [5] apply Pinch Analysis techniques to explore the performance of five different ORC structures including single and multi-pressure cycles to convert heat from process streams to power and observe that the carefully integrated ORCs significantly outperform steam cycles in terms of conversion efficiency. In a similar manner, Romeo et al. [29] use Pinch Analysis and simulation techniques

to address the integration of heat sources at different temperature levels with an ORC structure, while Hackl and Harvey [30] and Luo et al. [28] investigate ORC integration cases considering a pre-specified ORC structure and operating parameters as decision criteria to identify efficient matches.

The above works illustrate that there are many options that need to be considered simultaneously both at the heat source side (e.g. placement of heat exchangers with respect to the ORC) and the ORC itself, prior to identifying an overall system of optimum performance. Optimization-based ORC integration methods which exploit Pinch principles can address this challenge more efficiently as they are able to support a more systematic evaluation of the available decision options. To this end, Marechal and Kalitventzeff [6] proposed a method for the optimal insertion of ORC in industrial processes. The method is based on the analysis of the shape of the grand composite curve, combined with the use of the minimum exergy losses concept, heuristic rules and a cost optimization technique. The focus of the proposed developments is on the integration of the ORC vaporization and condensation sections. Hipolito-Valencia et al. [32, 33], Lira-Barragan et al. [34] and Chen et al. [35] develop flexible mathematical models by conceptualizing the heat transfer operations in the form of a superstructure and this is combined with process optimization. Developments also focus on identifying the heat exchanger network configuration, while the expansion section is not considered. Kapil et al. [36] introduce a co-generation targeting method that considers the optimization of pressure levels together with integration options for ORC and heat pumps as low grade heat utilization options. Kwak et al. [37] and Gutiérrez-Arriaga et al. [38] optimize the operation of a basic ORC structure with respect to the corresponding heat source, whereas Soffiato et al. [39] compare three different, pre-specified ORC structures through an optimization approach whereby the efficient matching

of the heat source is performed using comprise curves analysis. Note, that most of the reviewed works compare the performance of different working fluids using mainly one fluid in each system in their effort to improve the efficiency of the ORC through the exploitation of the heat sources.

The presented literature review shows that while most approaches for the design and integration of ORC employ pinch analysis, approaches based on optimization are also gaining attention in recent years. Despite the promising results obtained, the employed approaches are based on mathematical models which either focus on designing an optimum heat exchanger network around an ORC with pre-specified expansion and pumping characteristics or on comparing different, pre-specified ORC structures. The consideration of an overall model for the efficient integration of multiple heat sources at different temperature levels with an ORC that simultaneously exploits different structural features and working fluids has yet to be considered. In this work we propose the combined use of pinch analysis and mathematical programming to identify optimum ORC structures and working fluids for multiple heat sources, considering multiple heat exchange (evaporation and condensing), pressure and expansion options in interacting ORC cascades.

2. Problem definition

Plant operations in different industrial sectors often involve an extensive use of thermally supported processes where hot streams are cooled down by cold utilities and exhaust streams (i.e. flue gas, water condensates etc.) are discharged to the environment at diverse heat grade levels. Unused heat transferred to cold utilities or released to the environment can generally be defined

as waste heat. Converting waste heat to power through ORC would clearly have a positive effect on the overall energy efficiency of such plants.

The simultaneous existence of waste heat from multiple sources at different temperature levels makes conversion to power rather challenging for ORC which are mainly designed to serve one heat source at a time. More complex ORC cascades are necessary which are able to efficiently exploit multiple heat sources and to simultaneously maximize the waste heat utilization and the ORC power generation while minimizing the use of cooling utilities (as they also utilize power to drive auxiliary equipment). An indicative example of such a cascade is shown in Figure 1 which illustrates two ORC sharing two waste heat streams (WS_1 and WS_2) and one cold utility (*CU*). One of the ORC operates based entirely on WS_1 while the other exploits WS_1 at a lower temperature to increase the temperature of the working fluid (WF_2) prior to exploiting the second waste heat source (WS_2). An interesting feature is that the two cycles are likely to need different working fluids, while the CU needs to be shared to serve different cooling demands. Such a configuration is one of multiple different possible options which may include two or more independent ORC, one multi-pressure cascade and so forth in order to best exploit multiple heat sources. Additional decision options may include the type of working fluids to be used in each ORC, the operating conditions (e.g. inlet and outlet temperatures, pressures and flowrates) and the placement of the heat exchangers for waste heat extraction (e.g. the temperature and pressure levels where they will be placed into the ORC flowsheet). Clearly, this is a complex design problem calling for a systematic method to support the simultaneous design and fluid selection of ORC cascades suitable for multiple heat sources.

Figure 1: Schematic representation of an ORC system

In this work, the design of ORC cascades is approached as a process design problem where an inclusive and flexible ORC model is automatically evolved by an optimization algorithm supporting a) the identification of operating targets for optimum waste heat exploitation from multiple sources, and b) the determination of the process structural characteristics (i.e. number and connection of different equipment), of the type of working fluid used in each structure and of the operating conditions that best match the identified targets. In formal mathematical terms we consider a set of waste heat streams *WS* that have to be cooled, and a set of working fluids *WF* that have to be heated to a thermodynamic state capable to produce power in an expansion process. For each waste heat stream *i*, the flowrate of each working fluid *j* (of properties β , κ , $c^{wf}_{p,\mathrm{vap}_p}$, c^{wf}_{p,liq_p} , Cp^{ig}_p , P^{sat}_p), the heat load as well as the supply and target temperatures are considered as decision parameters that need to be specified. In some cases the heat content of waste heat streams cannot be completely transferred to working fluids, hence residues of heat loads have to be removed by auxiliary cooling. It is assumed that auxiliary cooling is available from a set of cold utilities *CU* (i.e. water, air). The objective is to maximize the power output using equipment for subcritical ORC operation embedded in an ORC cascade. Each cascade is defined as a process consisting of a heat extraction, a power generation, a condensation and a liquid pressurization section. These four sections represent the building blocks used to synthesize ORC cascades. A vaporizer, a turbine, a condenser and a pump in the corresponding sections comprise the simplest possible cascade (i.e. a typical ORC) which may evolve to more complex forms through the use of different numbers and interconnections of equipment. Furthermore, pure fluids are only considered as working fluids. Under these assumptions the design problem can be defined as follows:

For given:

- Process operating conditions of waste heat streams, i.e., supply and target-temperatures, flowrates and heat capacities,
- Set of working fluids, their thermo-physical properties, maximum number of SORC processes,
- Cold utilities supply and target temperatures,
- Minimum temperature difference ΔT_{min} between heat source and heat sink streams.

Determine:

The number and structure of SORC cascades, operating conditions, number and type of working fluids, quantity and type of auxiliary cooling utilities which maximize the power output.

3. Proposed targeting and design model

3.1 Heat extraction section

Here we propose a model to ensure feasible heat transfer between the waste heat streams, the working fluids and the cold utilities in the heat extraction section of the ORC. Heat transfer in case of multiple heat sources is illustrated in an enthalpy – temperature diagram (Figure 2).

Figure 2: Enthalpy-temperature diagram of heat extraction section of ORC system

The heat extraction section of Figure 2 corresponds to multiple heat sources hence dealing with multiple pinch points. It is obviously much different to an ORC applied on a single heat source that deals with one pinch point. A pinch point can be considered as a bottleneck that limits heat transfer from *WS* to *WF*. When pure fluids in subcritical thermodynamic states are employed in the ORC system the emergence of a pinch point-cannot be avoided. However, its location can be adjusted to attain maximum power generation from the available heat. This can be achieved by

the selection of an appropriate working fluid and by adjusting the structure and operating conditions of the ORC.

A feasible heat transfer is defined by the second law of thermodynamics which states that heat can only be spontaneously transferred from a source that is at a higher temperature than the sink. To define a model for feasible heat transfer from source (waste streams) to sink (working fluids, cold utilities) the entire temperature range is partitioned into temperature intervals based on the procedure proposed by Linnhoff and Flower [26] for a pre-specified minimum temperature ΔT_{min}. The method considers two types of temperature intervals: the hot and the cold. The proposed procedure represents this method through a flexible mathematical model which consists of three main stages which are analyzed below:

- The determination of the boundary values of hot and cold temperature intervals.
- The determination of whether a stream is present in the hot or the cold temperature interval.
- The implementation of the energy balance.

3.1.1 Determination of boundary values

The procedure evaluates the boundary values for two sets of temperature intervals: hot and cold from known values of supply and target temperatures of waste heat streams and cold utility streams, and values of working fluid condensation, saturation and superheated temperatures. As mentioned previously in the problem definition section, the operating conditions which include the operating temperatures of *WF* (condensation, vaporization and superheating) of the ORC are unknowns which need to be determined through an iterative procedure during optimization. To determine the boundary values of each temperature interval in each iteration the procedure of

Linnhoff and Flower [26] should be adopted to handle variations in the ORC operating temperatures as follows:

i) To evaluate the boundary values of the hot temperature intervals (*TI*), the *WS* temperature values ($T_{in_i}^{ws}, T_{out_i}^{ws}$) are constant. Supply ($T_{in_u}^{cu}$) and targeted temperatures ($T_{out_u}^{cu}$) of *CU* temperature values are increased by ΔT_{min}. Condensing ($T_{cond_j}^{wf}$), vaporization ($T_{sat_j}^{wf}, T_{sat_j}^{wf}+1$), and superheated ($T_{sh_j}^{wf}$) temperatures of *WF* are also increased by ΔT_{min}. The concept of $T_{sat_j}^{wf}+1$ is explained later in the manuscript. To determine the hot *TI* it is necessary to sort temperatures in descending order from highest to lowest.

ii) To evaluate cold *TI*, the evaluated temperature values of hot temperature intervals are reduced by ΔT_{min}.

The following set of equations is used to automatically generate boundary values for *TI* in each iteration (an example illustrating the use of the equations follows in Figure 3):

$$\begin{aligned}\theta_k^{hot} = {} & \sum_{i\in WS} y_{in_{i,k}}^{ws}\cdot T_{in_i}^{ws} + \sum_{i\in WS} y_{out_{i,k}}^{ws}\cdot T_{out_i}^{ws} + \sum_{j\in WF} y_{cond_{j,k}}^{wf}\cdot\left(T_{cond_j}^{wf}+\Delta T_{\min}\right) \\ & + \sum_{j\in WF} y_{satliq_{j,k}}^{wf}\cdot\left(T_{sat_j}^{wf}+\Delta T_{\min}\right) + \sum_{j\in WF} y_{satvap_{j,k}}^{wf}\cdot\left(T_{sat_j}^{wf}+\Delta T_{\min}+1\right) \\ & + \sum_{j\in WF} y_{sh_{j,k}}^{wf}\cdot\left(T_{sh_j}^{wf}+\Delta T_{\min}\right) + \sum_{u\in CU} y_{in_{u,k}}^{cu}\cdot\left(T_{in_u}^{cu}+\Delta T_{\min}\right) \\ & + \sum_{u\in CU} y_{out_{u,k}}^{cu}\cdot\left(T_{out_u}^{cu}+\Delta T_{\min}\right) \qquad \forall k\in TI\end{aligned} \tag{1}$$

$$\begin{aligned}& \sum_{i\in WS} y_{in_{i,k}}^{ws} + \sum_{i\in WS} y_{out_{i,k}}^{ws} + \sum_{j\in WF} y_{cond_{j,k}}^{wf} + \sum_{j\in WF} y_{satliq_{j,k}}^{wf} \\ & + \sum_{j\in WF} y_{satvap_{j,k}}^{wf} + \sum_{j\in WF} y_{sh_{j,k}}^{wf} + \sum_{u\in CU} y_{in_{u,k}}^{cu} + \sum_{u\in CU} y_{out_{n,k}}^{cu} = 1 \qquad \forall k\in TI\end{aligned} \tag{2}$$

$$\theta_k^{hot} - \theta_{k+1}^{hot} \geq 0 \qquad \forall k \in TI \tag{3}$$

$$\sum_{k \in TI} y_{in_{i,k}}^{ws} = 1 \qquad \forall i \in WS \tag{4a}$$

$$\sum_{k \in TI} y_{out_{i,k}}^{ws} = 1 \qquad \forall i \in WS \tag{4b}$$

$$\sum_{k \in TI} y_{cond_{j,k}}^{wf} = 1 \qquad \forall j \in WF \tag{4c}$$

$$\sum_{k \in TI} y_{satliq_{j,k}}^{wf} = 1 \qquad \forall j \in WF \tag{4d}$$

$$\sum_{k \in TI} y_{satvap_{j,k}}^{wf} = 1 \qquad \forall j \in WF \tag{4e}$$

$$\sum_{k \in TI} y_{sh_{j,k}}^{wf} = 1 \qquad \forall j \in WF \tag{4f}$$

$$\sum_{k \in TI} y_{in_{u,k}}^{cu} = 1 \qquad \forall j \in WF \tag{4g}$$

$$\sum_{k \in TI} y_{out_{u,k}}^{cu} = 1 \qquad \forall j \in WF \tag{4h}$$

$$y_{in_{i,k}}^{ws}, y_{out_{i,k}}^{ws}, y_{cond_{j,k}}^{wf}, y_{satliq_{j,k}}^{wf}, y_{satvap_{j,k}}^{wf}, y_{sh_{j,k}}^{wf}, y_{in_{u,k}}^{cu}, y_{out_{n,k}}^{cu} \in \{0,1\} \; \forall i \in WS, \forall j \in WF, \forall u \in CU, \forall k \in TI \tag{4i}$$

After determining the boundary values of the hot temperature intervals, the boundary temperatures of the cold temperature intervals are evaluated as follows:

$$\theta_k^{cold} = \theta_k^{hot} - \Delta T_{\min} \qquad \forall k \in TI \tag{5}$$

Figure 3 illustrates the heat extraction section of an ORC system in a temperature interval diagram.

Figure 3: Illustration of heat extraction section in temperature interval diagram

The ORC consists of 3 waste heat streams (red lines), 2 independent SORC cascades (green lines) and a cold utility (blue line). It is assumed that waste heat streams bounded by supply ($T_{in_i}^{ws}$) and targeted ($T_{out_i}^{ws}$) temperature have constant heat capacity values. Each green line (corresponding to the *WF*) consists of 3 segments which represent 3 different phases of the working fluid in the heat extraction section: 1) the liquid phase of *WF j* is bounded by condensation $T_{cond_j}^{wf}$ and vaporization $T_{sat_j}^{wf}$ temperature, 2) the liquid – vapor phase of the *WF j* is bounded by temperatures $T_{sat_j}^{wf}$ and $T_{sat_j}^{wf}$ +1, 3) the vapor phase of the *WF j* is bounded by temperatures $T_{sat_j}^{wf}$ +1 and $T_{sh_j}^{wf}$. The temperature bounds imposed in each phase require the introduction of the following constraints:

$$T_{cond_j}^{wf} - T_{sat_j}^{wf} \le 0 \qquad \forall j \in WF \tag{6a}$$

$$T_{sat_j}^{wf} + 1 - T_{sh_j}^{wf} \le 0 \qquad \forall j \in WF \tag{6b}$$

Moreover, general constraints are introduced to set up upper and lower bounds for the temperature of the *WF*:

$$T_{sh_j}^{wf} - T_{in_i}^{ws} - T_{\max} \le 0 \qquad \forall i \in WS;\ \forall j \in WF \tag{7a}$$

$$T_{sh_j}^{wf} - T_{c_j} \le 0 \qquad \forall j \in WF \tag{7b}$$

$$T_{c_j} = \sum\nolimits_{p \in PWF} Tcr_p \cdot \delta_{j,p}^{wf} \qquad \forall j \in WF, \forall p \in PWF \tag{7c}$$

$$T_{b_j} - T_{cond_j}^{wf} \le 0 \qquad \forall j \in WF \tag{7d}$$

$$T_{b_j} = \sum\nolimits_{p \in PWF} Tbl_p \cdot \delta_{j,p}^{wf} \qquad \forall j \in WF, \forall p \in PWF \tag{7e}$$

$$T_{sat_j}^{wf} + 1 - T_{sh_j}^{wf} \leq 0 \qquad \forall j \in WF \tag{7f}$$

$$T_{out_u}^{cu} + \Delta T_{\min} - T_{cond_j}^{wf} \leq 0 \qquad \forall j \in WF, \forall u \in CU \tag{7g}$$

The above model accounts for different *WF* as decision parameters together with the conditions of the ORC. The working fluids are part of set *PWF* hence *WF j* which enables the optimum matching of the *WS* heat can be selected simultaneously with the ORC characteristics as follows:

$$\sum_{p \in PWF} \delta_{j,p}^{wf} = 1 \qquad \forall j \in WF \tag{8a}$$

$$\delta_{j,p}^{wf} \in \{0,1\} \tag{8b}$$

It is assumed that the liquid phase of the *WF* can be approximated by constant heat capacity within each temperature interval. The same holds for the two phase and superheating states. The heat capacity of the liquid and superheating states are estimated based on the average of the starting and ending temperatures of the respective phase. According to thermodynamic theory the heat capacity throughout phase-change of pure fluids has an infinite value, because temperature is constant during vaporization. To apply this concept for liquid-vapor phase-change, it is assumed that by receiving heat equal to the heat of vaporization the *WF* will increase its temperature by 1K. Hence, the heat capacity during phase-change is equal to the heat of vaporization. This mathematical manipulation enables the use of the heat capacity concept in the two phase region and is common practice in numerous cases of heat integration [40].

3.1.2 Presence of a stream in a hot or cold interval

The calculation of the energy balance for each temperature interval requires the determination of the heat load for each stream. To automatically determine whether *WS i* is present in the hot

temperature interval *k*, the supply temperature of *WS i* has to be higher than the average temperature of the hot *TI k*, while the targeted temperature has to be lower than average temperature of *TI k*. An average temperature of the hot *TI k* is defined as follows:

$$\xi_k^{hot} = \frac{\theta_k^{hot} + \theta_{k+1}^{hot}}{2} \qquad \forall k \in TI \tag{9}$$

Equation (9) enables the introduction of three zones as shown in Equation (10a). The first zone denotes that the average temperature of the hot *TI k* is higher than the inlet temperature of *WS i*. The second zone denotes that average temperature is between the supply and targeted temperatures of *WS i*. The third zone denotes that the average temperature of *TI k* is below the targeted temperature of *WS i*. If $w_{i,k,l}^{ws}$ for the second zone is equal to 1 the *WS i* is present in *TI k*, whereas in all other cases it is not. This is represented by the following equations:

$$w_{i,k,l}^{ws} = \begin{cases} 1,\ T_{in_i}^{ws} < \xi_k^{hot} \le T_{\max} \\ 1,\ T_{out_i}^{ws} < \xi_k^{hot} \le T_{in_i}^{ws}; \\ 1,\ T_{\min} < \xi_k^{hot} \le T_{out_i}^{ws} \end{cases} \qquad \forall i \in WS; \forall k \in TI; \forall l \in WSEG \tag{10a}$$

$$\sum\nolimits_{l \in WSEG} w_{i,k,l}^{ws} = 1 \qquad \forall i \in WS; \forall k \in TI \tag{10b}$$

$$w_{i,k,l}^{ws} \in \{0,1\} \tag{10c}$$

The heat load of *WS i* in each hot temperature interval can be estimated as follows:

$$Q_k^{ws} = \sum\nolimits_{i \in WS} F_i^{ws} w_{i,k,2}^{ws} \cdot c_{p_i}^{ws} \cdot \left(\theta_k^{hot} - \theta_{k+1}^{hot}\right) \qquad \forall k \in TI \tag{11a}$$

$$Q_k^{ws} \ge 0 \qquad \forall k \in TI \tag{11b}$$

The average temperature of cold a *TI k* is defined as follows:

$$\xi_k^{cold} = \frac{\theta_k^{cold} + \theta_{k+1}^{cold}}{2} \qquad \forall k \in TI \qquad (12)$$

Figure 3 indicates that:

- The liquid phase of *WF j* is present in the cold *TI k* if the condensing temperature $T_{cond_j}^{wf}$ is lower than the average temperature of cold the *TI k*, and if the vaporization temperature $T_{sat_j}^{wf}$ is higher than the average temperature of the cold *TI k*.
- The liquid-vapor phase of *WF j* is present in the cold *TI k* if the vaporization temperature $T_{sat_j}^{wf}$ is lower than the average temperature of the cold *TI k*, and if $T_{sat_j}^{wf} + 1$ is higher than the average temperature of the cold *TI k*.
- The superheating phase of *WF j* is present in cold *TI k*, if temperature $T_{sat_j}^{wf} + 1$ is lower than average temperature of the cold *TI k*, and if the superheating temperature $T_{sh_j}^{wf}$ is higher than the average temperature of cold *TI k*.

To determine whether *WF j* is present in the cold *TI k* five zones are introduced through Equation (13a). The first zone denotes that the average temperature of *TI k* is higher than the superheating temperature of *WF j*. The second zone denotes that *WF j* at average temperature of cold *TI k* is superheated. The third zone denotes that that *WF j* at the average temperature of cold *TI k* undergoes phase-change. The fourth zone denotes that *WF j* at the average temperature of the cold *TI k* is in liquid phase. The fifth zone denotes that the average temperature of *TI k* is below the condensing temperature of *WF j*. In the second zone, if $w_{j,k,h}^{wf}$ is equal to 1 then *WF j* is

present in the superheated state in *TI k*. In the third zone, if $w_{j,k,h}^{wf}$ is equal to 1 then *WF j* is present in the vapor-liquid state in *TI k*. In the fourth zone, if $w_{j,k,h}^{wf}$ is equal to 1 then *WF j* is present as liquid in *TI k*.

$$w_{j,k,h}^{wf} = \begin{cases} 1, & T_{sh_j}^{wf} < \xi_k^{cold} \le T_{\max} \\ 1, & T_{sat_j}^{wf} + 1 < \xi_k^{cold} \le T_{sh_j}^{wf} \\ 1, & T_{sat_j}^{wf} < \xi_k^{cold} \le T_{sat_j}^{wf} + 1 \\ 1, & T_{cond_j}^{wf} < \xi_k^{cold} \le T_{sat_j}^{wf} \\ 1, & T_{\min} < \xi_k^{cold} \le T_{cond_j}^{wf} \end{cases} ; \qquad \forall j \in WF; \forall k \in TI; \forall h \in WFSG \tag{13a}$$

$$\sum\nolimits_{h \in WFSG} w_{j,k,h}^{wf} = 1 \qquad \forall j \in WF; \forall k \in TI \tag{13b}$$

$$w_{j,k,h}^{wf} \in \{0,1\} \tag{13c}$$

The heat load of the *WF* streams in each cold *TI* can be estimated as follows:

$$Q_k^{wf} = \sum\nolimits_{j \in WF} F_j^{wf} \cdot \left[\sum\nolimits_{h \in PWFSG} w_{j,k,h}^{wf} \cdot CP_{j,k,h}^{wf} \cdot \left(\theta_k^{cold} - \theta_{k+1}^{cold} \right) \right] \quad \forall k \in TI; \forall h \in PWFSG \subseteq WFSG = \{2,3,4\} \tag{14a}$$

$$Q_k^{wf} \ge 0 \qquad \forall k \in TI \tag{14b}$$

The heat load of *WF* streams in each cold *TI k* depends on heat capacities of the available working fluids, the flowrate and the temperature difference. The heat capacity of *WF j* in *TI k* can be defined as follows:

$$\begin{aligned} CP_{j,k,2}^{wf} &= \sum\nolimits_{p \in PWF} c_{p,\mathrm{sh}_p}^{wf} \cdot \delta_{j,p}^{wf} \\ CP_{j,k,3}^{wf} &= \sum\nolimits_{p \in PWF} c_{p,\mathrm{vap}_p}^{wf} \cdot \delta_{j,p}^{wf} \\ CP_{j,k,4}^{wf} &= \sum\nolimits_{p \in PWF} c_{p,liq_p}^{wf} \cdot \delta_{j,p}^{wf} \end{aligned} \qquad \forall j \in WF; \forall k \in TI \tag{15}$$

To determine whether the *CU* stream *u* is present in cold *TI k*, the starting temperature of the *CU* has to be lower than the average temperature of the cold *TI k*, while the ending temperature has to be higher than the average temperature of the cold *TI k*. Therefore, three zones are introduced again as shown in Equation (16). The first zone denotes that the average temperature of *TI k* is above the outlet temperature of *CU u*. The second zone denotes that the average temperature of *TI k* is between inlet and outlet temperature of *CU u*. The third zone denotes that average temperature of *TI k* is below the inlet temperature of *CU u*. In the second zone, if $w_{\mathrm{u},k,s}^{cu}$ is equal to 1 then the *CU u* is present in *TI k*.

$$w_{\mathrm{u},k,s}^{cu}=\begin{cases}1,\ T_{out_u}^{cu}<\xi_k^{cold}<T_{\max}\\ 1,\ T_{in_u}^{cu}<\xi_k^{cold}<T_{out_u}^{cu}\\ 1,\ T_{\min}<\xi_k^{cold}<T_{in_u}^{cu}\end{cases};\qquad \forall u\in CU;\forall k\in TI;\forall s\in CUSG \tag{16a}$$

$$\sum\nolimits_{s\in CUSG} w_{u,k,s}^{cu}=1 \qquad \forall u\in CU;\forall k\in TI \tag{16b}$$

$$w_{u,k,s}^{cu}=\{0,1\} \tag{16c}$$

The heat load of *CU* streams in each cold temperature interval *k* can be estimated as follows:

$$Q_k^{cu}=\sum\nolimits_{u\in CU} F_u^{cu}\cdot w_{\mathrm{u},k,2}^{cu}\cdot c_{p_u}^{cu}\cdot\left(\theta_k^{cold}-\theta_{k+1}^{cold}\right)\ \forall k\in TI \tag{17a}$$

$$Q_k^{cu}\geq 0 \qquad \forall k\in TI \tag{17b}$$

3.1.3 Energy balance

When the presence of the streams and the heat load for each stream in each *TI k* is determined, the energy balance for each *TI k* is set up based on the transshipment model proposed by

Papoulias and Grossmann [41]. The heat flows of *WS* which enter into a *TI k* exchange heat with the *WF* and the *CU* streams (Figure 4). During heat exchange a part of the heat is transferred to the *WF* and the *CU* streams. The remainders of the heat flows are lead to the next lower *TI*.

Figure 4: Heat balance of temperature interval

Based on Figure 4 the energy balance for each *TI k* is defined as follows:

$$R_k - R_{k+1} = Q_k^{ws} - \sum_{i \in WS} \sum_{j \in WF} Q_{i,j,\mathrm{k}}^{ws-wf} - \sum_{i \in WS} \sum_{u \in CU} Q_{i,\mathrm{u},\mathrm{k}}^{ws-cu} \qquad \forall k \in TI \tag{18a}$$

$$R_k \geq 0 \qquad \forall k \in TI \tag{18b}$$

The heat exchanged between the *WS* and the *WF* in *TI k* is determined as follows:

$$\sum_{i \in WS} \sum_{j \in WF} Q_{i,j,k}^{ws-wf} = Q_k^{wf} \qquad \forall k \in TI \tag{19a}$$

$$Q_{i,j,k}^{ws-wf} \geq 0 \qquad \forall i \in WS, \forall j \in WF, \forall k \in TI \tag{19b}$$

Heat exchanged between *WS* and *CU* in *TI k* is defined as:

$$\sum_{i \in WS} \sum_{u \in CU} Q_{i,\mathrm{u},k}^{ws-cu} = Q_k^{cu} \qquad \forall k \in TI \tag{20a}$$

$$Q_{i,j,k}^{ws-cu} \geq 0 \qquad \forall i \in WS, \forall u \in CU, \forall k \in TI \tag{20b}$$

It is worth noting that the heat extraction section of an ORC system does not have heating requirements. This can be defined by setting heat flow to the first *TI* to zero:

$$R_1 = 0 \tag{21a}$$

The cooling is required in the heat extraction section of an ORC system to cool down waste heat streams to target temperatures. This is provided by cold utilities, therefore heat flow from last temperature interval *k* is equal to zero, and this can be defined as follows:

$$R_{NTI+1} = 0 \tag{21b}$$

Equations (1) – (21) define the heat extraction section of the ORC system.

3.2 Power generation section

The work generated in the polytropic expansion process by an expansion turbine is defined as follows:

$$W_{turb_j} = \sum_{j\in WF} \eta_{turb_j} \cdot F_j^{wf} \frac{\gamma_j}{\gamma_j - 1} Z_{sh_j} \cdot R_{gas} \cdot T_{sh_j}^{wf} \left[1 - \left(\frac{PCD_j}{PST_j} \right)^{\frac{\gamma_j - 1}{\gamma_j}} \right] \qquad \forall j \in WF \tag{22a}$$

$$PCD_j = \sum_{p\in PWF} \delta_{j,p} \cdot P_p^{cond} \qquad \forall j \in WF \tag{22b}$$

$$PST_j = \sum_{p\in PWF} \delta_{j,p} \cdot P_p^{sat} \qquad \forall j \in WF \tag{22c}$$

$$\frac{\gamma_j - 1}{\gamma_j} = \frac{R_{gas}}{CP_j^{turb}} \qquad \forall j \in WF \tag{22d}$$

$$CP_j^{turb} = \sum_{p\in PWF} c_{p,\mathrm{sh}_p}^{wf} \cdot \delta_{j,p}^{wf} \qquad \forall j \in WF \tag{22e}$$

The temperature at the turbine outlet can be estimated by following expression:

$$T_{turbout_j}^{wf} = T_{sh_j}^{wf} \frac{Z_{sh_j}}{Z_{turbout_j}} \left(\frac{PCD_j}{PST_j} \right)^{\frac{\gamma_j - 1}{\gamma_j}} \qquad \forall j \in WF \tag{22f}$$

3.3 Heat removal section

Thermal energy that is extracted and is not transformed into power has to be removed from the system by *CU* in the heat removal section. Typical cooling options include air coolers and water recirculation towers. Removed heat may be calculated as follows:

$$Q_j^{hr} = F_j^{wf} \cdot \left[CPSH_j \cdot \left(T_{turbout_j}^{wf} - T_{cond_j}^{wf} \right) + HCD_j \right] \qquad \forall j \in WF \tag{23a}$$

$$CPSH_j = \sum\nolimits_{p \in PWF} c_{p,\mathrm{sh}_p}^{wf} \cdot \delta_{j,p}^{wf} \qquad \forall j \in WF \tag{23b}$$

$$HCD_j = \sum\nolimits_{p \in PWF} \delta_{j,p}^{wf} \cdot \Delta H_{cond_p}^{wf} \left(T_{cond_j}^{wf} \right) \qquad \forall j \in WF \tag{23c}$$

The power requirements for cooling process depend on the design of the cooling system, the amount of heat removed, the operating conditions and cold utility properties [42]. The power requirement for the heat removal process is defined as follows:

$$W_{cond_j} = \lambda_j \cdot Q_j^{hr} \qquad \forall j \in WF \tag{23d}$$

3.4 Liquid pressurization section

After condensation, the saturated liquid has to be pumped to the operating pressure associated with the heat extraction section. The corresponding power requirement is determined as follows:

$$W_{pump_j} = \frac{F_j^{wf} \cdot v_j^{sat} \left[PST_j - PCD_j \right]}{\eta_{pump_j}} \qquad \forall j \in WF \tag{24a}$$

$$v_j^{sat} = \sum\nolimits_{p \in PWF} \delta_{j,p} \cdot v_p^{sat} \qquad \forall j \in WF \tag{24b}$$

3.5 Objective function for ORC optimization

In this paper the goal is to maximize power production from the available waste heat streams. The total net power output is defined as follows:

$$W_{net} = \sum_{j \in WF} \left(W_{turb_j} - W_{cond_j} - W_{pump_j} \right) \tag{25}$$

The objective function is therefore defined as follows:

$$\min \Phi = -W_{net} \tag{26}$$

4. Optimization model and approach

The above Equations (1) – (26) form a mixed integer nonlinear program (MINLP) which will be solved to identify the optimum ORC configuration together with the most appropriate combination of working fluid that minimize the proposed objective function. Since the MINLP formulation contains many non-convex nonlinear, bilinear and tri-linear terms, we develop an optimization model of reduced complexity. The Adams and Sherali method [43] is used to linearize bilinear terms consisted of a binary and a continuous variable. The outline of the method is given in Appendix A. The temperature-dependent thermo-physical properties are approximated using piecewise linear functions. The method is outlined in Appendix B. The problem is solved using the Branch and Bound algorithm proposed by Tawarmalani and Sahinidis [44]. The method constructs convex under-estimators for the non-convex objective function and inequality constraints by relaxing the nonlinear equality constraints, replacing them with less stringent linear equality constraints or a set of two convex inequalities. The method is incorporated in the BARON algorithm [44].

4.1 Heat extraction section

In Equation (1) the product between binary variables $y^{wf}_{cond_{j,k}}$ and $T^{wf}_{cond_j}$ can be linearized using the method proposed by Adams and Sherali [43]. The method introduces the new variables $z^{wf}_{cond_{j,k}} = y^{wf}_{cond_{j,k}} \cdot T^{wf}_{cond_j}$, $z^{wf}_{satliq_{j,k}} = y^{wf}_{satliq_{j,k}} \cdot T^{wf}_{sat_j}$, $z^{wf}_{satvap_{j,k}} = y^{wf}_{satvap_{j,k}} \cdot T^{wf}_{sat_j}$ and $z^{wf}_{sh_{j,k}} = y^{wf}_{sh_{j,k}} \cdot T^{wf}_{sh_j}$. Equation (1) is therefore transformed to a set of linear equations. Equation (10a) determines the zone *l* in which the average temperature of the hot *TI k* is assigned. The linearization is approached using the method proposed by Balas [45] based on the following set of linear equations:

$$\xi^{hot}_k - \sum_{l \in WSEG} \psi^{ws}_{i,k,l} = 0 \qquad \forall i \in WS; \forall k \in TI; \qquad (27a)$$

$$\psi^{ws}_{i,k,1} \le T^{ws}_{out_i} \cdot w^{ws}_{i,k,1} \qquad \forall i \in WS; \forall k \in TI \qquad (27b)$$

$$-\psi^{ws}_{i,k,1} \le -T_{\min} \cdot w^{ws}_{i,k,1} \qquad \forall i \in WS; \forall k \in TI \qquad (27c)$$

$$\psi^{ws}_{i,k,2} \le T^{ws}_{in_i} \cdot w^{ws}_{i,k,2} \qquad \forall i \in WS; \forall k \in TI \qquad (27d)$$

$$-\psi^{ws}_{i,k,2} \le T^{ws}_{out_i} \cdot w^{ws}_{i,k,2} \qquad \forall i \in WS; \forall k \in TI \qquad (27e)$$

$$\psi^{ws}_{i,k,3} \le T_{\max} \cdot w^{ws}_{i,k,3} \qquad \forall i \in WS; \forall k \in TI \qquad (27f)$$

$$-\psi^{ws}_{i,k,3} \le T^{ws}_{in_i} \cdot w^{ws}_{i,k,3} \qquad \forall i \in WS; \forall k \in TI \qquad (27g)$$

The heat load of the hot streams in each hot *TI* given by Equation (11a) is a bilinear expression because the binary variable $w^{ws}_{i,k,2}$ is multiplied by the continuous variables θ^{hot}_k and θ^{hot}_{k+1}. The flowrate F^{ws}_i and heat capacity $c^{ws}_{p_i}$ are constants. The expression is linearized using the Adams

and Sherali [43] method by introducing the new variable $wt_{i,k} = w^{ws}_{i,k,2} \cdot \theta^{hot}_{k}$. Equation (13a) determines the zone *h* in which the average temperature of the cold *TI k* is assigned. The linearization is approached by the method of Balas [45] as follows:

$$\xi^{cold}_{k} - \sum\nolimits_{h \in WFSG} \psi^{ws}_{i,k,h} = 0 \qquad \forall j \in WF; \forall k \in TI \qquad (28a)$$

$$-\psi^{wf}_{j,k,1} \le -T_{\min} \cdot w^{wf}_{j,k,1} \qquad \forall j \in WF; \forall k \in TI \qquad (28b)$$

$$\psi^{wf}_{j,k,1} \le T^{wf}_{cond_j} \cdot w^{wf}_{j,k,1} \qquad \forall j \in WF; \forall k \in TI \qquad (28c)$$

$$\psi^{wf}_{j,k,2} \le T^{wf}_{sat_j} \cdot w^{wf}_{j,k,2} \qquad \forall j \in WF; \forall k \in TI \qquad (28d)$$

$$-\psi^{wf}_{j,k,2} \le -T^{wf}_{cond_j} \cdot w^{wf}_{j,k,2} \qquad \forall j \in WF; \forall k \in TI \qquad (28e)$$

$$\psi^{wf}_{j,k,3} \le \left(T^{wf}_{sat_j} + 1\right) \cdot w^{wf}_{j,k,3} \qquad \forall j \in WF; \forall k \in TI \qquad (28f)$$

$$-\psi^{wf}_{j,k,3} \le -T^{wf}_{sat_j} \cdot w^{wf}_{j,k,3} \qquad \forall j \in WF; \forall k \in TI \qquad (28g)$$

$$\psi^{wf}_{j,k,4} \le T^{wf}_{sh_j} \cdot w^{wf}_{j,k,4} \qquad \forall j \in WF; \forall k \in TI \qquad (28h)$$

$$-\psi^{wf}_{j,k,4} \le -\left(T^{wf}_{sat_j} + 1\right) \cdot w^{wf}_{j,k,4} \qquad \forall j \in WF; \forall k \in TI \qquad (28i)$$

$$-\psi^{wf}_{j,k,5} \le -T^{wf}_{sh_j} \cdot w^{wf}_{j,k,5} \qquad \forall j \in WF; \forall k \in TI \qquad (28j)$$

$$\psi^{wf}_{j,k,5} \le T_{\max} \cdot w^{wf}_{j,k,5} \qquad \forall j \in WF; \forall k \in TI \qquad (28k)$$

Equations (28c) – (28j) contain binary and continuous variables generating the bilinear terms $T^{wf}_{cond_j} \cdot w^{wf}_{j,k,1}$, $T^{wf}_{sat_j} \cdot w^{wf}_{j,k,2}$, $T^{wf}_{cond_j} \cdot w^{wf}_{j,k,2}$, $\left(T^{wf}_{sat_j}+1\right) \cdot w^{wf}_{j,k,3}$, $T^{wf}_{sat_j} \cdot w^{wf}_{j,k,3}$, $T^{wf}_{sh_j} \cdot w^{wf}_{j,k,4}$, $\left(T^{wf}_{sat_j}+1\right) \cdot w^{wf}_{j,k,4}$ and $T^{wf}_{sh_j} \cdot w^{wf}_{j,k,5}$. These terms are linearized by the method of Adams and Sherali [43].

The heat load of *WF* streams for each *TI* is given by Equation (14a). The bilinear term $w^{wf}_{j,k,h} \cdot CP^{wf}_{j,k,h}$ (right side) can be substituted by a new variable $wcp^{wf}_{j,k,h}$ and linearized using the Adams and Sherali [43] method. The *WF* heat load in each *TI k* can be calculated from:

$$Q^{wf}_k = \sum_{j \in WF} F^{wf}_j \cdot \left[\sum_{h \in PWFSG} wcp^{wf}_{j,k,h} \cdot \left(\theta^{cold}_k - \theta^{cold}_{k+1} \right) \right] \quad \forall k \in TI; \forall h \in PWFSG \subseteq WFSG = \{2,3,4\} \tag{29}$$

The heat capacity of each zone *h* is expressed Equation (15) as a sum of the bilinear terms $c^{wf}_{p,\mathrm{sh}_p} \cdot \delta^{wf}_{j,p}$, $c^{wf}_{p,\mathrm{vap}_p} \cdot \delta^{wf}_{j,p}$ and $c^{wf}_{p,liq_p} \cdot \delta^{wf}_{j,p}$ which are linearized by the Adams and Sherali [43] method. The heat capacity of the *WF* in the superheating zone can therefore be expressed as follows:

$$c^{wf}_{p,\mathrm{sh}_p}\left(\bar{T}^{wf}_{sh_j}\right)\left(T^{wf}_{sh_j} - T^{wf}_{sat_j} - 1\right) - Cp^{ig}_p\left(\bar{T}^{wf}_{sh_j}\right) \cdot \left(T^{wf}_{sh_j} - T^{wf}_{sat_j} - 1\right) - H^R_{sh_p}\left(\bar{T}^{wf}_{sh_j}\right) = 0 \quad \forall j \in WF, \forall p \in PWF \tag{30}$$

The ideal gas $Cp^{ig}_p\left(\bar{T}^{wf}_{sh_j}\right)$ dependence on temperature for the *WF* is a non-linear function which is approximated by a piecewise linear function given in Appendix B.

In this paper, we assume the use of a Virial equation of state (EoS) to estimate residual enthalpy and compressibility factors. A Virial EoS offers the advantage that compressibility factors and residuals enthalpies are defined by explicit functions, whereas other common EoS such as the

commonly used Peng – Robinson equation [46] functions are implicit. This considerably reduces complexity of problem [47]. The residual enthalpies for superheating are estimated using the second Virial coefficient. The residual enthalpy dependence on temperature for the considered *WF* is a non-linear function as expressed by Equation (34a).

$$H_{sh_p}^{R}\left(\bar{T}_{sh_j}^{wf}\right)=P_p^{sat}\cdot\beta_p^{sh} \qquad \forall p\in PWF \tag{31a}$$

$$\beta_p^{sh}=\alpha_{p,1}+\frac{2\alpha_{p,2}}{\bar{T}_{sh_j}^{wf}}+\frac{4\alpha_{p,3}}{\left(\bar{T}_{sh_j}^{wf}\right)^3}+\frac{9\alpha_{p,4}}{\left(\bar{T}_{sh_j}^{wf}\right)^8}+\frac{10\alpha_{p,5}}{\left(\bar{T}_{sh_j}^{wf}\right)^9} \qquad \forall p\in PWF \tag{31b}$$

The liquid vapor pressure, the coefficient β_p^{sh}, the heat capacity considered in the liquid-vapor phase change and the liquid heat capacity are non-linear functions of temperature hence they are approximated by piecewise linear functions given in Appendix B. Equation (16a) is similar to Equation (13a) hence linearizations are approached using the method of Balas [45] as follows:

$$\xi_k^{cold}-\sum\nolimits_{lu\in NCUSG}\psi_{u,k,lu}^{cu}=0 \qquad \forall u\in CU;\forall k\in TI \tag{32a}$$

$$\psi_{\mathrm{u},k,1}^{cu}\le T_{in_u}^{cu}\cdot w_{\mathrm{u},k,1}^{cu} \qquad \forall u\in CU;\forall k\in TI \tag{32b}$$

$$-\psi_{\mathrm{u},k,1}^{cu}\le -T_{\min}\cdot w_{u,k,1}^{cu} \qquad \forall u\in CU;\forall k\in TI \tag{32c}$$

$$\psi_{\mathrm{u},k,2}^{cu}\le T_{out_u}^{cu}\cdot w_{\mathrm{u},k,2}^{cu} \qquad \forall u\in CU;\forall k\in TI \tag{32d}$$

$$-\psi_{u,k,2}^{cu}\le -T_{in_u}^{cu}\cdot w_{u,k,2}^{cu} \qquad \forall u\in CU;\forall k\in TI \tag{32e}$$

$$\psi_{\mathrm{u},k,3}^{cu}\le T_{\max}\cdot w_{\mathrm{u},k,3}^{cu} \qquad \forall u\in CU;\forall k\in TI \tag{32f}$$

$$-\psi_{u,k,3}^{cu} \le -T_{out_u}^{cu} \cdot w_{u,k,3}^{cu} \qquad \forall u \in CU; \forall k \in TI \qquad (32g)$$

The heat load of the *CU* streams is given by Equation (17a). Term $w_{\mathrm{u},k,2}^{cu} \cdot c_{p_u}^{cu}$ is substituted by a new variable $wcp_{\mathrm{u},k,2}$ and linearized using the Adams and Sherali [43] method. After this transformation the heat load of the *CU* can be calculated as follows:

$$Q_k^{cu} = \sum_{u \in CU} F_u^{cu} \cdot wcp_{\mathrm{u},k} \cdot \left(\theta_k^{cold} - \theta_{k+1}^{cold}\right) \qquad \forall k \in TI \qquad (33)$$

4.2 Power generation section

The power generation in each turbine is presented by the set of Equations (22a-22e). The turbine efficiency is considered constant and the compressibility factors $Z_{turbout_j}$ and Z_{sh_j} are estimated using a Virial EOS as follows:

$$Z_{sh_j} = 1 + \frac{B_{sh_j}}{R \cdot T_{sh_j}} \cdot PST_j \qquad \forall j \in WF \qquad (34a)$$

$$B_{sh_j} = \sum_{p \in PWF} \delta_{j,p} \cdot \kappa_{sh_p} \qquad \forall j \in WF \qquad (34b)$$

$$\kappa_{sh_p} = \alpha_{p,1} + \frac{\alpha_{p,2}}{T_{sh_j}} + \frac{\alpha_{p,3}}{T_{sh_j}^3} + \frac{\alpha_{p,4}}{T_{sh_j}^8} + \frac{\alpha_{p,5}}{T_{sh_j}^9} \qquad \forall p \in PWF \qquad (34c)$$

$$Z_{turbout_j} = 1 + \frac{B_{turbout_j}}{R \cdot T_{turbout_j}^{wf}} \cdot PCD_j \qquad \forall j \in WF \qquad (34d)$$

$$B_{turbout_j} = \sum_{p \in PWF} \delta_{j,p} \cdot \kappa_{turbout_p} \qquad \forall j \in WF \qquad (34e)$$

$$\kappa_{turbout_p} = \alpha_{p,1} + \frac{\alpha_{p,2}}{T_{turbout_j}} + \frac{\alpha_{p,3}}{T^3_{turbout_j}} + \frac{\alpha_{p,4}}{T^8_{turbout_j}} + \frac{\alpha_{p,5}}{T^9_{turbout_j}} \qquad \forall p \in PWF \tag{34f}$$

The second Virial coefficients κ_{sh_p} and $\kappa_{turbout_p}$ are also non-linear function of temperature approximated by piecewise linear function given in Appendix B: Terms $\delta_{j,p} \cdot P_p^{cond}$, $\delta_{j,p} \cdot P_p^{sat}$ and $c^{wf}_{p,\mathrm{sh}_p} \cdot \delta^{wf}_{j,p}$ are linearized by the Adams and Sherali [43] method. The heat capacity in Equations (22d) - (22e) is estimated in the same manner as the heat capacity of the superheating zone and defined using the average temperature in the turbine inlet and outlet, as follows:

$$c^{wf}_{p,sht_p} \cdot \left(T^{wf}_{sh_j} - T_{turbout_j}\right) - Cp^{ig}_p\left(\bar{T}^{wf}_{turb_j}\right) \cdot \left(T^{wf}_{sh_j} - T_{turbout_j}\right) - H^R_{turb_p}\left(\bar{T}^{wf}_{turb_j}\right) = 0 \qquad \forall j \in WF, p \in PWF \tag{35a}$$

$$\bar{T}^{wf}_{turb_j} = \frac{T^{wf}_{sh_j} + T_{turbout_j}}{2} \qquad \forall j \in WF \tag{35b}$$

$$H^R_{turbout_p}\left(\bar{T}^{wf}_{turb_j}\right) = P^{sat}_p \cdot \beta^{shturb}_p \qquad \forall p \in PWF \tag{35c}$$

$$\beta^{shturb}_p = \alpha_{p,1} + \frac{2\alpha_{p,2}}{\bar{T}^{wf}_{turb_j}} + \frac{4\alpha_{p,3}}{\left(\bar{T}^{wf}_{turb_j}\right)^3} + \frac{9\alpha_{p,4}}{\left(\bar{T}^{wf}_{turb_j}\right)^8} + \frac{10\alpha_{p,5}}{\left(\bar{T}^{wf}_{turb_j}\right)^9} \qquad \forall p \in PWF \tag{35d}$$

The $Cp^{ig}_p\left(\bar{T}^{wf}_{turb_j}\right)$ and β^{shturb}_p are approximated by piecewise linear function given in Appendix B. The power generation of the turbines in Equation (22a) is transformed to the following equality expression:

$$W_{turb,j} PST_j^{\frac{\gamma-1}{\gamma}} - \eta_{turb,j} \cdot CP^{turb}_j\left(\bar{T}^{twf}_{turb_j}\right) \cdot \frac{B_{sh_j}\left(T_{sh_j}\right)}{R_{gas}} \cdot PST_j \left[PST_j^{\frac{\gamma-1}{\gamma}} - PCD_j^{\frac{\gamma-1}{\gamma}} \right] = 0 \quad \forall j \in WF \tag{36}$$

4.3 Heat removal section

The removed heat can be estimated using Equations (23a)-(23c). Terms $c_{p,\mathrm{sh}_p}^{wf} \cdot \delta_{j,p}^{wf}$ and $\delta_{j,p}^{wf} \Delta H_{cond_p}^{wf}\left(T_{cond_j}^{wf}\right)$ are linearized using the Adams and Sherali [43] method. $\Delta H_{cond_p}^{wf}\left(T_{cond_j}^{wf}\right)$ is approximated by a piecewise linear function given in Appendix B. Moreover, heat capacity estimated as follows:

$$c_{p,shturb_p}^{wf} \cdot \left(T_{turbout_j} - T_{cond_j} - 1\right) - Cp_p^{ig}\left(\bar{T}_{turbavg}\right) \cdot \left(T_{turbout_j} - T_{cond_j} - 1\right) - H_{turbout_p}^{R}\left(\bar{T}_{turbout_j}^{wf}\right) = 0 \qquad \forall j \in WF, p \in PWF \tag{37a}$$

$$\beta_p^{shturbout} = \alpha_{p,1} + \frac{2\alpha_{p,2}}{\bar{T}_{turbout_j}^{wf}} + \frac{4\alpha_{p,3}}{\left(\bar{T}_{turbout_j}^{wf}\right)^3} + \frac{9\alpha_{p,4}}{\left(\bar{T}_{turbout_j}^{wf}\right)^8} + \frac{10\alpha_{p,5}}{\left(\bar{T}_{turbout_j}^{wf}\right)^9} \qquad \forall p \in PWF \tag{37b}$$

$$H_{turbout_p}^{R}\left(\bar{T}_{turbout_j}^{wf}\right) = P_p^{cond} \cdot \beta_p^{shturbout} \qquad \forall p \in PWF \tag{37c}$$

$$\bar{T}_{turbout_j}^{wf} = \frac{T_{turbout_j} + T_{cond_j} + 1}{2} \qquad \forall j \in WF \tag{37d}$$

4.4 Liquid pressurization section

The pumping power requirements are calculated by Equation (24a). The bilinear terms $\delta_{j,p} \cdot \upsilon_p^{sat}$ in Equation (24b) are linearized using the Adams and Sherali [43] method. The specific molar volume is estimated using the Rackett equation [48] as follows:

$$\upsilon_p^{sat} = \frac{R_{gas} \cdot Tcr_p}{P_{C_p}} Z_{C_p}^{\left(1 - \frac{T_{cond_j}^{wf}}{Tcr_p}\right)^{2/7}} = V_{C_p} \cdot Z_{C_p}^{\left(1 - \frac{T_{cond_j}^{wf}}{Tcr_p}\right)^{2/7}} \qquad \forall p \in PWF \tag{38}$$

Term $Z_{C_p}^{\left(1 - \frac{T_{cond_j}^{wf}}{T_C}\right)^{2/7}}$ is expressed as a piecewise linear function given in Appendix B:

5. Calculation methodology

The step-by-step procedure required to develop the proposed model based on the above set of equations involves the following:

Step 1: Define waste heat streams (supply and target temperatures, flowrates, and heat capacities).

Step 2: Define cold utilities (fluids, supply and target temperatures).

Step 3: Select potential working fluids.

Step 4: Approximate temperature dependant thermo-physical properties of working fluids (β, κ, $c^{wf}_{p,\mathrm{vap}_p}$, c^{wf}_{p,liq_p}, Cp^{ig}_p, P^{sat}_p) by piecewise linear functions (Appendix B).

Step 5: Introduce new variables to Eq.(1) $z^{wf}_{cond_{j,k}}$, $z^{wf}_{satliq_{j,k}}$, $z^{wf}_{satvap_{j,k}}$ and $z^{wf}_{sh_{j,k}}$. Use Eqs. (A.1) – (A.4) to establish new variables linear relationships with binary ($y^{wf}_{cond_{j,k}}$, $y^{wf}_{satliq_{j,k}}$, $y^{wf}_{satvap_{j,k}}$ and $y^{wf}_{sh_{j,k}}$) and continuous ($T^{wf}_{cond_j}$, $T^{wf}_{sat_j}$, $T^{wf}_{sat_j}$ and $T^{wf}_{sh_j}$) variables.

Step 6: Specify linear constrains given by Eqs.(2) – (9).

Step 7: Transform set of nonlinear constraints given by Eq.(10a) to set of linear constrains using Eqs. (27a) – (27g).

Step 8: Specify linear constraints given by Eq. (10b).

Step 9: The heat load of WS in TI *k* given by Eq. (11a), is linearized by introducing new variable $wt_{i,k}$ and establishing relationship between it and binary $w^{ws}_{i,k,2}$ and continuous variable θ^{hot}_k using Eqs. (A.1) – (A.4).

Step 10: Introduce linear constraints given by Eq. (12).

Step 11: Transform the set of nonlinear constraints given by Eq. (13a) to a new set of equations given by Eqs. (28a) – (28k). Introduce new variables: $wT^{wf}_{cond_{j,k,1}} = T^{wf}_{cond_j} \cdot w^{wf}_{j,k,1}$, $wT^{wf}_{j,k,2} = T^{wf}_{sat_j} \cdot w^{wf}_{j,k,2}$

, $wT^{wf}_{j,k,2} = T^{wf}_{cond_j} \cdot w^{wf}_{j,k,2}$, $wT^{wf}_{j,k,3} = T^{wf}_{sat_j} \cdot w^{wf}_{j,k,3}$, $wT^{wf}_{j,k,3} = T^{wf}_{sat_j} \cdot w^{wf}_{j,k,3}$, $wT^{wf}_{j,k,4} = T^{wf}_{sh_j} \cdot w^{wf}_{j,k,4}$, $wT^{wf}_{j,k,4} = T^{wf}_{sat_j} \cdot w^{wf}_{j,k,4}$ and $wT^{wf}_{j,k,5} = T^{wf}_{sh_j} \cdot w^{wf}_{j,k,5}$. Establish relationships between new variables with corresponding binary and continuous variables using Eqs. (A.1) – (A.4).

Step 12: V**:** Introduce heat load of *WF* for each *TI k* Eq. (29). Establish linear relationships between $wcp^{wf}_{j,k,h}$ and corresponding binary $w^{wf}_{j,k,h}$ and continuous variables ($CP^{wf}_{j,k,h}$) using Eqs. (A.1)-(A.4).

Step 13: Linearize Eq. (15) by introducing new variables: $c\delta^{wf}_{j,p} = c^{wf}_{p,\mathrm{sh}_p} \cdot \delta^{wf}_{j,p}$, $c\delta^{wf}_{j,p} = c^{wf}_{p,\mathrm{vap}_p} \cdot \delta^{wf}_{j,p}$ and $c\delta^{wf}_{j,p} = c^{wf}_{p,liq_p} \cdot \delta^{wf}_{j,p}$. Relationships between new variables and corresponding binary and continuous variables are given by Eqs. (A.1) – (A.4).

Step 14: Introduce bilinear constraints given by Eq. (30), which evaluate heat capacity of superheating.

Step 15: Transform the set of nonlinear constraints given by Eq.(16a) to a set of linear constrains using Eqs. (32a) – (32g).

Step 16: Introduce the linear constraints given by Eq. (16b).

Step 17: Term $w^{cu}_{\mathrm{u},k,2} \cdot c^{cu}_{p_u}$ in Eq. (17a) is substituted by new variable $wcp_{\mathrm{u},k,2}$. Establish relationships between new variables with corresponding binary ($w^{cu}_{\mathrm{u},k,2}$) and continuous ($c^{cu}_{p_u}$) variables using Eqs.(A.1)-(A.4).

Step 18: Introduce the heat load of cold utilities given by Eq. (17a).

Step 19: Introduce the energy balance using Eqs. (18a)-(21b)

Step 21: Linearize Eqs. (22b) and (22c) by introducing new variables $P\delta_{j,p}{}^{cond}$ and by applying Eqs. (A.1)-(A.4).

Step 22: Linearize Eq.(22e) in the same manner as in Step 13.

Step 23: Introduce bilinear constraints given by Eq. (35a), which evaluate the heat capacity of superheating.

Step 24: Introduce bilinear constraints given by Eq.(22d).

Step 25: Linearize Eq. (34b) and (34e) by introducing new variables and applying Eqs. (A.1) – (A.4).

Step 26: Introduce nonlinear constraints of bilinear type given by Eqs. (34a) and (34d)

Step 27: Introduce nonlinear constraints given by Eqs. (22f) and (36).

Step 28: Linearize Eqs. (23b) and (23c) by introducing new variables and applying Eqs. (A.1)-(A.4)

Step 29: Introduce bilinear constraints given by Eq. (37a), which evaluate the heat capacity of superheating.

Step 30: Introduce nonlinear constrainst of trlinear type for heat removal given by Eq. (23a)

Step 31: Introduce power for condensation given by Eqs. (23d).

Step 32: Linearize Eq. (24b) by introducing new variables and applying Eqs. (A.1)-(A.4)

Step 33: Introduce the power required for pumping trough nonlinear constraints of trilinear type given by Eq. (24a).

Step 34: Introduce the objective function given by Eq. (25).

6. Implementation

This section illustrates the proposed approach with a case study. The aim is to determine the maximum power production from waste heat carried by two waste streams by minimizing objective function (Equation 26). The inlet and outlet temperatures of hot streams as well as heat load available in each stream are given in Table 1.

Table 1: Waste heat stream data

Cooling in the process is assumed to be performed by water of inlet temperature of 298.15K and targeted temperature of 313.15 K, and heat capacity of 4.0 kJ/kg/K. Selection of the working fluids is performed based on Tchanche et al. [49] classification of working fluids for subcritical operations. The working fluids considered as decision options during process optimization are the following: 1) 1,1,1,2-Tetrafluoroethane, 2) 1,1,1,3,3-Pentafluoropropane, 3) Hexane, 4) Ethanol, 5) Benzene, 6) Toluene, and 7) Tribrommethane. The required thermo-physical properties are obtained from the DIPPR database [50]. Also, it is assumed that up to four SORC processes can be used at maximum, so up to four working fluids may be employed as part of the set *WF*. The continuous decision variables include the molar flowrates of the working fluids (F_j^{wf}), the molar flowrates of the cold utility (F_u^{cu}), the condensing temperatures of the working fluids ($T_{cond_j}^{wf}$), the vaporization temperatures of working fluid streams ($T_{sat_j}^{wf}$), and the superheating temperatures of the working fluids ($T_{sh_j}^{wf}$). The discrete decision variables are based on binary variables used to select working fluids from the available options.

The lower bounds for $T_{cond_j}^{wf}$, $T_{sat_j}^{wf}$, and $T_{sh_j}^{wf}$ are equal to the maximum value between the normal boiling temperature of the selected working fluids (T_{b_j}) and the inlet temperature of the cooling medium ($T_{in_u}^{cu}$) increased by $\Delta T_{\min}$,i.e. $\max(T_{b_j}, T_{in_u}^{cu}) + \Delta T_{\min}$. The upper bounds for the same temperatures are equal to the critical temperatures of the working fluids (T_{c_j}) that are selected each time. In this case study, F_j^{wf} is in the range between 0 and 1 kmol/s and F_u^{cu} is in the range between 0 and 150 kg/s. The power required to remove 1 kW of heat from working fluid stream *j*

is assumed constant, at 0.01 kW per kW of removed heat [42]. The coefficients for piecewise linear function approximations are given in table B.1 of Appendix B.

7. Results and discussion

The original problem consists of 708 nonlinear and 138 linear constraints with 196 binary variables. For the original MINLP it took more than 24 hr of CPU time to find the first feasible point. The linearization of the original problem reduced number of nonlinear constraints to 80, of which only four are exponential, while all others are bilinear or trilinear. As a result of the linarization, the number of linear constrains increased to 3096 and the number of binary variables to 396. The resulting MINLP is solved in less than 21 min of CPU time on a desktop PC (Intel(R) Core(TM) i5 CPU 3.33 GHz, with 8.00 GB of RAM) using GAMS with BARON Solver [51]. The optimum number of ORC cascades is 2 as shown in Table 2, which also illustrates the optimum values for the decision variables. To illustrate the advantages of the proposed solution, Table 2 also contains the optimum values of the decision variables in case that only one SORC system is considered.

Table 2: Case study results

Based on the results presented in Table 2, the net power production in the case of two SORC is 14.7 % higher than in the case of the single SORC. Also, 25.8 % more heat is extracted from the waste heat streams in the case of two SORC. The thermal efficiency in the case of two SORC is approximately 1.5 % lower than in the case of one SORC. This behavior is reasonable because in the case of the two SORC the extracted heat contains higher quantity of low grade heat (heat at lower temperature) which leads to lower thermal efficiency. On the other hand, in the case of two SORC the higher net power output supports a 5 % higher exergy efficiency. In both cases, the condensation temperature of benzene is equal to the normal boiling temperature, whereas for

1,1,1,3,3-Pentafluoropropane it is set to the lower value shown in Table 2. The vaporization temperature for benzene and 1,1,1,3,3-Pentafluoropropane is lower than their critical temperature. The superheated temperatures are higher by only 1K than the vaporization temperatures. This is expected because Benzene and 1,1,1,3,3-Pentafluoropropane are so called dry fluids hence superheating is avoided. Finally, the system of two SORC includes higher condensation and pumping requirements than the single SORC, which are compensated by higher power generation in the turbine.

Figures 5a and 5b illustrate the composite curves in the heat extraction section when the single SORC and double SORC systems are employed with their corresponding working fluids. In Figure 5a, segment 1 shows the cooling of the waste heat streams using cold utility. Segments 2 and 3 indicate the heating of the working fluid until the states of saturated liquid and saturated vapor, respectively. The pinch temperature which occurs at 428.15 K imposes a limitation on the quantity of heat that can be transferred from the waste streams to the working fluid. By employing the two SORCs the pinch temperature occurs at 353.2 K hence there is a much better exploitation of the available heat above the pinch. This is clearly illustrated in Figure 5b where segment 1 represents cooling of waste heat streams by cold utility. Segment 2 represents heat transfer from waste heat streams to cold utility and 1,1,1,3,3-Pentafluoropropane. Segment 3 represents heat transfer from waste heat streams to 1,1,1,3,3-Pentafluoropropane. Segment 4 represents heating of 1,1,1,3,3-Pentafluoropropane to the state of saturated liquid, as well as heating of benzene. Segment 5 represents heating of 1,1,1,3,3-Pentafluoropropane from saturated liquid to saturated vapor. Segment 6 represents heating of benzene to the saturated liquid whereas segment 7 shows the phase change of benzene from saturated liquid to saturated vapor. Figure 5b clearly shows that the amount of heat lost to the cold utility is very small compared to

Figure 5a. Furthermore, the existence of two working fluids allows the extraction of more heat during phase change and less sensible heating in each one of the two cascades.

Figure 5: Composite curves for heat extraction section of a) single SORC, b) two SORC

Figure 5b indicates that there are more temperature intervals than in the case of Figure 5a, however this does not necessitate a considerably complex or capital intensive heat exchanger network (HEN). Figures 6 and 7 illustrate the HEN for the cases of the one and two SORC. Both networks consist of three *WS*-*WF* and two *WS*-*CU* heat exchangers. The size of the *CU* heat exchangers will be smaller in Figure 7 due to the much lower cooling load. On the other hand, heat exchangers 2 and 3 in the case of two SORC (Figure 7) transfer most of the additional heat load compared to the case of one SORC, but they operate at a much higher temperature difference (i.e., 54 K and 21.9 K for heat exchangers 2 and 3). Despite the extraction of higher amounts of heat in Figure 7, the heat exchanger area is unlikely to be higher than in the case of one SORC where both heat exchangers 2 and 3 operate at a difference of approximately 10 K. The split of streams observed in Figure 7 increases the complexity of the stream network compared to Figure 6, however this is not expected to have a significant impact on capital expenditures since the heat exchanger area is by far the most important feature.

Figure 6: Heat exchanger network for heat extraction section of single SORC

Figure 7: Heat exchanger network for heat extraction section of two SORC

Figures 8 and 9 illustrate how the two HENs are connected to the entire SORC configuration. In Figure 9, the SORC at the top exploits part of the heat that cannot be efficiently utilized from the SORC at the bottom. Compared to the configuration in Figure 8, there is a need for an additional pump and an additional turbine in Figure 9, whereas the overall condenser area will also be

slightly higher in Figure 9 due to the higher cooling loads. The additional capital costs for this equipment are likely to be compensated by reductions induced in heat exchanger areas due to higher temperature differences, as noted previously. Overall, the higher power output achieved in the case of two SORC and the qualitative indications about the expected capital costs compared to the case of one SORC appear to be promising. Based on Quoilin [52] et al., the cost of ORC equipment depends on volumetric flowrates, heat transfer area and power required for pumping the working fluid. All these parameters can be evaluated for the results obtained in the presented study so as to identify the lower cost design.

Figure 8: Illustration of single SORC system

Figure 9: Illustration of two SORC systems

8. Conclusions

This paper has presented an approach to design SORC systems which are able to efficiently exploit more than one heat sources using multiple ORC cascades. The approach also includes the simultaneous selection of working fluids for each cascade from a pool of pre-selected working fluids. The design problem follows an MINLP formulation where maximum net power output is chosen as the objective function. Partial linearization of the initial MINLP is performed to reduce the computational effort by considerably reducing the number of nonlinear constraints. The problem is solved using the global deterministic optimization algorithm proposed by Tawarmala and Sahinidis [44] and the optimum solution consists of a system with two SORC which operate using Benzene and 1,1,1,3,3-Pentafluoropropane as working fluids. The obtained results indicate that by using two ORC cascades with different working fluids it is possible to avoid heat transfer limitations caused in a single cascade and considerably increase the extracted heat. A qualitative analysis of the impact that the two ORC cascades have on capital costs, indicates that the ability of proposed system to operate at much higher temperature differences than the single SORC.

This will have a positive effect on the required heat exchange areas which take up a large percentage of the overall system costs. The proposed approach maximizes a thermodynamic performance criterion. Future work will address economic criteria as objective functions. This would require significant research efforts towards an extended approach, which would balance additional complexity from potentially highly non-linear equipment design models and cost functions with appropriate accuracy of predictions to enable design decisions.

Acknowledgments

Aleksandar Grujić and Mirjana Kijevčanin are grateful to Ministry of Education, Science and Technological Development (project III 45019 , TR 34011, OI 172063) for support.

Nomenclature

Indices:

h - zone in which of working fluid stream *j* is present

i – waste heat stream

j – working fluid employed in ORC system

k – temperature interval

l – zone in which of waste heat stream *i* is present

p – potential working fluid for ORC system

s - zone in which of cold utility *u* is present

u – cold utility

Sets:

CU – set of cold utilities

CUSG - set of zones cold utility *u*

PWF – set of potential working fluids

TI – set of temperature intervals

WFSG - set of zones working fluid *j*

WSEG – set of zones for waste heat stream *i*

WS – set of waste heat streams

WF – set of employed working fluids

Parameters:

$c_{p_u}^{cu}$ - heat capacity of cold utility *u (kJ/kmol/K)*

$c_{p_i}^{ws}$ - heat capacity of waste stream *i (kJ/kmol/K)*

F_i^{ws} - mole flowrate of waste stream *i (kmol/sec)*

NTI – total number of temperature intervals

P_{c_p} - critical pressure of working fluid p (Pa)

R_{gas} - universal gas constant *(kJ/kmol/K)*

Tbl_p - boiling temperature of promising working fluid *p* at 1atm (K)

Tcr_p - critical temperature of promising working fluid *p* (K)

$T_{in_u}^{cu}$ - cold utility *u* supply temperature (K)

$T_{in_i}^{ws}$ - waste heat stream *i* supply temperature (K)

T_{max} – maximum temperature *(K)*

T_{min} – minimum temperature *(K)*

T_0 - surrounding temperature 298 K

$T_{out_u}^{cu}$ - cold utility *u* ending temperature (K)

$T_{out_i}^{ws}$ - waste heat stream *j* target temperature (K)

V_{Cp} - critical molar volume of promising working fluid *p* (m^3/kmol)

Z_{C_p} - critical temperature of working fluid, *p* (K)

$\alpha_{p,m}$ - parameter *n* of second Virial coefficient of promising working fluid *p*

$\Delta Tmin$ – minimum temperature approach (K)

$\eta_{pump,j}$ - pump efficiency for working fluid stream *j (%)*

$\eta_{turb,j}$ - turbine efficiency for working fluid stream *j (%)*

λ_j - power required to remove 1kW of heat from working fluid stream *j*

Variables:

CP_j^{turb} - average heat capacity between inlet and outlet of turbine for working fluid *j kJ/kmol/K)*

$CPSH_j$ - average heat capacity between outlet of turbine and condensation temperature for working fluid *j kJ/kmol/K)*

$CP_{j,k,h}^{wf}$ - heat capacity of working fluid *j* in TI *k* in zone *h (kJ/kmol/K)*

Cp_p^{ig} - ideal gas heat capacity of promising working fluid p *(kJ/kmol/K)*

c_{p,liq_p}^{wf} - liquid heat capacity of potential working fluid *p(kJ/kmol/K)*

$c_{p,\mathrm{vap}_p}^{wf}$ - liquid-vapor heat capacity of potential working fluid *p(kJ/kmol/K)*

c_{p,sh_p}^{wf} - super heating heat capacity of potential working fluid *p (kJ/kmol/K)*

F_u^{cu} - mole flowrate of cold utility *u (kmol/sec)*

F_j^{wf} - mole flowrate of working fluid stream *j (kg/sec)*

HCD_j - heat of condensation for working fluid j (kJ/kmol)

$H_{sh_p}^R$ - residual enthalpy for superheated phase of promising working fluid p (kJ/kmol)

T_{c_j} - critical temperature of working fluid *j* (K)

P_p^{sat} - vaporization pressure of potential working fluid *p (Pa)*

P_p^{cond} - condensation pressure of potential working fluid *p (Pa)*

PCD_j - condensation pressure of working fluid *j (Pa)*

PST_j - vaporization pressure of working fluid *j (Pa)*

Q_k^{ws} - heat which waste heat streams exchange in temperature interval *k*(KW)

$Q_{i,j,\mathrm{k}}^{ws-wf}$ - heat exchanged between waste heat stream *i* and working fluid stream *j*(KW)

$Q_{i,\mathrm{u},\mathrm{k}}^{ws-cu}$ - heat exchanged between waste heat stream *i* and cold utility *u* (KW)

Q_k^{wf} - heat load which working fluid streams receive in temperature interval *k*(KW)

Q_k^{cu} - heat load which cold utilities receive in temperature interval *k* (KW)

Q_j^{hr} - *heat* removed from working stream *j* during condensation (KW)

R_k - heat flow to temperature interval *k* (KW)

$T_{cond_j}^{wf}$ - condensing temperature of working fluid stream *j* (K)

$T_{sat_j}^{wf}$ - vaporization temperature of working fluid stream *j* (K)

$T_{sh_j}^{wf}$ -superheating temperature of working fluid stream *j* (K)

$T_{turbout_j}^{wf}$ - turbine outlet temperature of working fluid stream *j* (K)

T_{c_j} - critical temperature of working fluid j (K)

T_{b_j} - boiling temperature of working fluid j at 1 atm (K)

$\overline{T}_{sh_j}^{wf}$ - average temperature between vaporization and superheating temperature *(K)*

W_{cond_j} - work required by auxiliary units in condensation process (kW)

W_{pump_j} - work required to pressurize working fluid *j* from condensing to vaporization pressure (kW)

W_{turb_j} - work produced in turbine by expanding working fluid stream *j* (kW)

Z_{sh_j} - compressibility factor at working fluid stream *j* at superheating temperature

$Z_{turbout_j}$ - compressibility factor at working fluid stream *j* at turbine outlet temperature

γ_j - polytropic expansion coefficient of working fluid stream j

κ_{sh_p} , $\kappa_{turbout_p}$ - second Virial coefficients of promising working fluid p (m^3/kmol)

ΔEx_{loss} - exergy loss during heat exchange between waste heat streams and working fluid streams *(kW)*

$\Delta H^{wf}_{cond_j}$ - specific heat requited for phase change of saturated vapor to saturated liquid (kW)

θ^{hot}_k - boundary temperature of hot temperature interval *k* (K)

θ^{cold}_k - boundary temperature of cold temperature interval *k* (K)

v_j^{sat} saturation molar volume of working fluid stream *j*

ξ^{hot}_k - average temperature of hot temperature interval *k* (K)

ξ^{cold}_k - average temperature of cold temperature interval *k* (K)

υ_p^{sat} - saturation molar volume of promising working fluid *p* (m^3/kmol)

Binary variables

$y^{ws}_{in_{i,k}}$ - if 1 supply temperature of waste heat stream *i* is boundary temperature of temperature interval *k*

$y^{ws}_{out_{i,k}}$ - if 1 targeting temperature of waste heat stream *i* is boundary temperature of temperature interval *k*

$y^{wf}_{cond_{j,k}}$ - if 1 condensing temperature of working fluid stream *j* is boundary temperature of temperature interval *k*

$y^{wf}_{satliq_{j,k}}$ - if 1 bubble temperature of working fluid stream *j* is boundary temperature of temperature interval *k*

$y^{wf}_{satvap_{j,k}}$ - if 1 dew temperature of working fluid stream *j* is boundary temperature of temperature interval *k*

$y^{wf}_{sh_{j,k}}$ - if 1 superheated temperature of working fluid stream *j* is boundary temperature of temperature interval *k*

$y^{cu}_{in_{u,k}}$ - if 1 inlet temperature of cold utility *u* is boundary temperature interval *k*

$y^{cu}_{out_{u,k}}$ - if 1 outlet temperature of cold utility *u* is boundary temperature interval *k*

$w^{ws}_{i,k,l}$ - if 1 waste stream *i* is present in temperature interval *k* in zone *l*

$w^{wf}_{j,k,h}$ - if 1 working fluid *j* is present in temperature interval *k* in zone *h*

$w^{cu}_{u,k,s}$ - if 1 cold utility *u* is present in temperature interval *k* in zone *s*

$\delta^{wf}_{j,p}$ -if 1working fluid *j* is selected from potential working fluid *p*

Appendix A

The Adams and Sherali method introduces a new variable which is equal to a product of the binary (*bin*) and the continuous (*con*) variable $nv = bin \cdot con$. The new variable *nv* has to satisfy the following linear conditions.

$$nv \le bin \cdot con_{\max} \qquad \text{Eq. (A.1)}$$

$$nv = con \qquad \text{Eq. (A.2)}$$

$$nv \ge con - con_{\max}\left(1 - bin\right) \qquad \text{Eq. (A.3)}$$

$$nv \ge 0 \qquad \text{Eq. (A.4)}$$

Appendix B

Any nonlinear nonconvex function can be approximated by a set of piecewise linear functions as follows:

$$f(T)=\begin{cases} f^0+\alpha_1(T-A_1) & A_1\le T\le A_2 \\ f^0+\alpha_1(A_2-A_1)+\alpha_2(T-A_2) & A_2<T\le A_3 \\ f^0+\alpha_1(A_2-A_1)+\alpha_2(A_3-A_2)+\alpha_3(T-A_3) & A_3<T\le A_4 \\ f^0+\alpha_1(A_2-A_1)+\alpha_2(A_3-A_2)+\ldots+\alpha_n\gamma(T-A_n) & A_n<T\le A_{n+1} \end{cases} \quad \text{Eq. (B.1)}$$

$$f(T)=f^0+\sum_{i\in N}\alpha_i\tau_i \quad \text{Eq. (B.2)}$$

$$T=A_1+\sum\nolimits_{i\in N}\tau_i \quad \text{Eq. (B.3)}$$

$$\chi_i(A_{i+1}-A_i)\le\tau_i\le(A_{i+1}-A_i) \qquad \forall i\in\{1\} \quad \text{Eq. (B.4)}$$

$$\chi_i(A_{i+1}-A_i)\le\tau_i\le(A_{i+1}-A_i)\chi_{i-1} \qquad \forall i\in\{2,n-1\} \quad \text{Eq. (B.5)}$$

$$0\le\tau_i\le(A_n-A_{n-1})\chi_{i-1} \qquad \forall i\in\{n\} \quad \text{Eq.(B.6)}$$

$$\chi_{i+1}\le\chi_i \qquad \forall i\in\{1,n\} \quad \text{Eq. (B.7)}$$

$$\chi_i\in\{0,1\} \quad \text{Eq. (B.8)}$$

Table B.1: Coefficients for piecewise linear function approximations on thermophysical properties

Table B.1 (Continued)

References

[1] Liu X, Liang J, Xiang D, Yang S, Qian Y. A proposed coal-to-methanol process with CO_2 capture combined Organic Rankine Cycle (ORC) for waste heat recovery. J Clean Prod. 2016; 129: 53–64.

[2] Uusitalo A, Uusitalo V, Grönman A, Luoranen M, Jaatinen-Värri A. Greenhouse gas reduction potential by producing electricity from biogas engine waste heat using organic Rankine cycle. J Clean Prod. 2016; 127: 399-405.

[3] Walsh C, Thornley P. The environmental impact and economic feasibility of introducing an Organic Rankine Cycle to recover low grade heat during the production of metallurgical coke. J Clean Prod. 2012; 34: 29-37.

[4] HREII DEMO Observatory, EUpaper: ORC waste heat recovery in European energy Intensive industries, Project No. LIFE10/ENV/IT/000397. (Annex4.2. II PaperEU), European Union; 2013 http://www.hreii.eu/public/Annex%204.2.II%20EU%20paper%20def.pdf (Accessed 11/3/2016)

[5] DiGenova KJ, Botros BB, Brisson JG. Method for customizing an organic Rankine cycle to a complex heat source for efficient energy conversion, demonstrated on a Fischer Tropsch plant. Appl Energ. 2013;102:746-54.

[6] Marechal F, Kalitventzeff B. A methodology for the optimal insertion of organic Rankine cycles in industrial processes. 2nd International Symposium of Process Integration Dalhousie University. Halifax, Canada 2004.

[7] Saleh B, Koglbauer G, Wendland M, Fischer J. Working fluids for low-temperature organic Rankine cycles. Energy. 2007;32(7):1210-21.

[8] Heberle F, Bruggemann D. Exergy based fluid selection for a geothermal Organic Rankine Cycle for combined heat and power generation. Appl Therm Eng. 2010;30(11-12):1326-32.

[9] Hettiarachchia HDM, Golubovica M, Worek WM, Ikegami Y. Optimum design criteria for an Organic Rankine cycle using low-temperature geothermal heat sources. Energy. 2007;32(9):1698-706.

[10] Tchanche BF, Papadakis G, Lambrinos G, Frangoudakis A. Fluid selection for a low-

temperature solar organic Rankine cycle. Appl Therm Eng. 2009;29(11-12):2468-76.

[11] Papadopoulos AI, Stijepovic M, Linke P. On the systematic design and selection of optimal working fluids for Organic Rankine Cycles. Appl Therm Eng. 2010;30(6-7):760-9.

[12] Papadopoulos AI, Stijepovic M, Linke P, Seferlis P, Voutetakis S. Toward Optimum Working Fluid Mixtures for Organic Rankine Cycles using Molecular Design and Sensitivity Analysis. Ind Eng Chem Res. 2013;52(34):12116-33.

[13] Quoilin S, Declaye S, Tchanche BF, Lemort V. Thermo-economic optimization of waste heat recovery Organic Rankine Cycles. Appl Therm Eng. 2011;31(14-15):2885-93.

[14] Drescher U, Bruggemann D. Fluid selection for the Organic Rankine Cycle (ORC) in biomass power and heat plants. Appl Therm Eng. 2007;27(1):223-8.

[15] Victor RA, Kim JK, Smith R. Composition optimisation of working fluids for Organic Rankine Cycles and Kalina cycles. Energy. 2013;55:114-26.

[16] Mavrou P, Papadopoulos AI, Stijepovic MZ, Seferlis P, Linke P, Voutetakis S. Novel and conventional working fluid mixtures for solar Rankine cycles: Performance assessment and multi-criteria selection. Appl Therm Eng. 2015;75:384-96.

[17] Stijepovic MZ, Linke P, Papadopoulos AI, Grujic AS. On the role of working fluid properties in Organic Rankine Cycle performance. Appl Therm Eng. 2012;36:406-13.

[18] Bao JJ, Zhao L. A review of working fluid and expander selections for organic Rankine cycle. Renew Sust Energ Rev. 2013;24:325-42.

[19] Chen HJ, Goswami DY, Stefanakos EK. A review of thermodynamic cycles and working fluids for the conversion of low-grade heat. Renew Sust Energ Rev. 2010;14(9):3059-67.

[20] Lecompte S, Huisseune H, van den Broek M, Vanslambrouck B, De Paepe M. Review of organic Rankine cycle (ORC) architectures for waste heat recovery. Renew Sust Energ Rev.

2015;47:448-61.

[21] Mago PJ, Chamra LM, Srinivasan K, Somayaji C. An examination of regenerative organic Rankine cycles using dry fluids. Appl Therm Eng. 2008;28(8-9):998-1007.

[22] Yamada N, Mohamad MNA, Kien TT. Study on thermal efficiency of low- to medium-temperature organic Rankine cycles using HFO-1234yf. Renew Energ. 2012;41:368-75.

[23] Schuster A, Karellas S, Aumann R. Efficiency optimization potential in supercritical Organic Rankine Cycles. Energy. 2010;35(2):1033-9.

[24] Stijepovic MZ, Papadopoulos AI, Linke P, Grujic AS, Seferlis P. An exergy composite curves approach for the design of optimum multi-pressure organic Rankine cycle processes. Energy. 2014;69:285-98.

[25] Klemeš JJ. Process integration handbook. Cambridge:: Woodhead Publishing, 2013.

[26] Linhoff B, Flower JR. Synthesis of heat exchanger networks: I. Systematic generation of energy optimal networks AIChE Journal. 1978;24:10.

[27] Desai NB, Bandyopadhyay S. Process integration of organic Rankine cycle. Energy. 2009;34(10):1674-86.

[28] Luo XL, Zhang BJ, Chen Y, Mo SP. Heat integration of regenerative Rankine cycle and process surplus heat through graphical targeting and mathematical modeling technique. Energy. 2012;45(1):556-69.

[29] Romeo LM, Lara Y, Gonzalez A. Reducing energy penalties in carbon capture with Organic Rankine Cycles. Appl Therm Eng. 2011;31(14-15):2928-35.

[30] Hackl R, Harvey S. Applying process integration methods to target for electricity production from industrial waste heat using Organic Rankine Cycle (ORC) technology. World Renewable Energy Congress 2011 Linköping, Sweden 2011. p. 1716–23.

[31] Song J, Li Y, Gu CW, Zhang L. Thermodynamic analysis and performance optimization of an ORC (Organic Rankine Cycle) system for multi-strand waste heat sources in petroleum refining industry. Energy. 2014;71:673-80.

[32] Hipolito-Valencia BJ, Rubio-Castro E, Ponce-Ortega JM, Serna-Gonzalez M, Napoles-Rivera F, El-Halwagi MM. Optimal integration of organic Rankine cycles with industrial processes. Energ Convers Manage. 2013;73:285-302.

[33] Hipolito-Valencia BJ, Rubio-Castro E, Ponce-Ortega JM, Serna-Gonzalez M, Napoles-Rivera F, El-Halwagi MM. Optimal design of inter-plant waste energy integration. Appl Therm Eng. 2014;62(2):633-52.

[34] Lira-Barragan LF, Ponce-Ortega JM, Serna-Gonzalez M, El-Halwagi MM. Sustainable Integration of Trigeneration Systems with Heat Exchanger Networks. Ind Eng Chem Res. 2014;53(7):2732-50.

[35] Chen CL, Chang FY, Chao TH, Chen HC, Lee JY. Heat-Exchanger Network Synthesis Involving Organic Rankine Cycle for Waste Heat Recovery. Ind Eng Chem Res. 2014;53(44):16924-36.

[36] Kapil A, Bulatov I, Smith R, Kim JK. Site-wide low-grade heat recovery with a new cogeneration targeting method. Chem Eng Res Des. 2012;90(5):677-89.

[37] Kwak DH, Binns M, Kim JK. Integrated design and optimization of technologies for utilizing low grade heat in process industries. Appl Energ. 2014;131:307-22.

[38] Gutierrez-Arriaga CG, Abdelhady F, Bamufleh HS, Serna-Gonzalez M, El-Halwagi MM, Ponce-Ortega JM. Industrial waste heat recovery and cogeneration involving organic Rankine cycles. Clean Technol Envir. 2015;17(3):767-79.

[39] Soffiato M, Frangopoulos CA, Manente G, Rech S, Lazzaretto A. Design optimization of

ORC systems for waste heat recovery on board a LNG carrier. Energ Convers Manage. 2015;92:523-34.

[40] Kemp IC. Pinch Analysis and Process Integration: A User Guide on Process Integration for the Efficient Use of Energy. 2nd ed. Oxford, UK: Elsevier, 2007.

[41] Papoulias SA, Grossmann IE. A structural optimization approach in process synthesis—II: Heat recovery networks. Computers & Chemical Engineering. 1983;7(6):15.

[42] Seider WD, Seader JD, Lewin DR. Product and process design principles: synthesis, analysis, and evaluation. 2nd ed. New York: John Wiley and Sons, 2004.

[43] Adams WP, Sherali HD. Linearization Strategies for a Class of Zero-One Mixed Integer Programming Problems. Operations Research. 1990;38:217-26.

[44] Tawarmalani M, Sahinidis N. Convexification and Global Optimization in Continuous and Mixed-Integer Nonlinear Programming: Theory, Algorithms, Software, and Applications 1st ed. Dordrecht: Springer Science, 2002.

[45] Balas E. Disjunctive programming: Properties of the convex hull of feasible points. Discrete Appl Math. 1998;89(1-3):3-44.

[46] Peng DY, Robinson DB. A New Two-Constant Equation of State. Industrial and Engineering Chemistry Fundamentals. 1976;15(1):59-64.

[47] Smith JM, Van Ness HC, Abbott MM. Introduction to Chemical Engineering Thermodynamics. 7th ed. Boston: McGraw-Hill, 2005

[48] Rackett HG. Equation of state for saturated liquids. Journal of Chemical & Engineering Data 1970;15(4):514-7.

[49] Tchanche BF, Lambrinos Gr, Frangoudakis A, Papadakis G. Low-grade heat conversion into power using organic Rankine cycles – A review of various applications, Renewable and

Sustainable Energy Reviews, 2011; 15(8): 3963–3979

[50] Rowley RL, Wilding WV, Oscarson JL, Giles NF. DIPPR-801 data compilation of pure chemical properties. Provo, Utah: Design Institute for Physical Properties. Brigham Young University; 2011.

[51] Tawarmalani M, Sahinidis N. A polyhedral branch-and-cut approach to global optimization. Mathematical Programming. 2005; 103(2): 225-293.

[52] Quoilin S, Declaye S, Tchanche BF, Lemort V. Thermo-economic optimization of waste heat recovery Organic Rankine Cycles. Appl Therm Eng. 2011: 31(14–15): 2885–93.

List of Figures:

List of Tables:

List of Tables:

Table 2: Waste stream data

Name	Inlet temperature (K)	Outlet temperature (K)	Heat load (kW/K)
WS_1	678.15	358.15	25
WS_2	428.15	328.15	35

Table 2: Case study results

Variable	**One SORC**	**Two SORC**	
Working fluids	Benzene	Benzene	1,1,1,3,3-Pentafluoropropane
W_{net} , kW	1407.07	1613.97	
Heat Extracted, kW	8330.9	11305.1	
Thermal Efficiency, %	16.89	14.27	
Exergy Efficiency, %	34.01	39.01	
F_u^{cu} ,kg/sec	52.84	3.25	
F_j^{wf} ,$kmol/sec$	0.1820	0.1346	0.1545
$T_{cond_j}^{wf}$,K	353.2	353.2	308.15
$T_{sat_j}^{wf}$,K	550.15	550.15	416.2
$T_{sh_j}^{wf}$,K	551.15	551.15	417.2
W_{turb_j} , kW	1587.90	1162.76	700.56
W_{pump_j} , kW	110.00	68.13	85.20
W_{cond_j} , kW	70.83	44.10	51.92

Table B.1: Coefficients for piecewise linear function approximations on thermophysical properties

Property	*Working fluid*	*f°*	A_1	A_2	A_3
Cp_p^{ig}	1,1,1,2-Tetrafluoroethane	87.0811	308.15	444.5	561.3
Cp_p^{ig}	1,1,1,3,3-Pentafluoropropane	118.42	308.15	444.5	541.8
Cp_p^{ig}	Hexane	159.49	341.80	465.77	571.96
Cp_p^{ig}	Ethanol	74.70	351.40	437.40	557.8
Cp_p^{ig}	Benzene	99.49	353.24	455.84	575.55
Cp_p^{ig}	Toluene	135.83	383.78	461.00	589.7
Cp_p^{ig}	Tribrommethane	79.54	422.35	503.13	583.91
P_p^{sat} , P_p^{cond} (Pa)	1,1,1,2-Tetrafluoroethane	0.8866e6	308.15	327.35	350.16
P_p^{sat} , P_p^{cond}	1,1,1,3,3-Pentafluoropropane	0.2128e6	308.15	341.27	376.63
P_p^{sat} , P_p^{cond}	Hexane	0.1013e6	341.88	391.53	441.57
P_p^{sat} , P_p^{cond}	Ethanol	0.1013e6	351.44	410.89	454.62
P_p^{sat} , P_p^{cond}	Benzene	0.1013e6	353.24	429.02	499.24
P_p^{sat} , P_p^{cond}	Toluene	0.1013e6	383.78	451.50	527.10
P_p^{sat} , P_p^{cond}	Tribrommethane	0.1013e6	422.35	525.65	611.96
β_p^{sh} , β_p^{shturb}	1,1,1,2-Tetrafluoroethane	-1.64	308.15	365.90	480.91
β_p^{sh} , β_p^{shturb}	1,1,1,3,3-Pentafluoropropane	-3.02	308.15	377.80	481.53
β_p^{sh} , β_p^{shturb}	Hexane	-4.85	341.8	421.22	542.05
β_p^{sh} , β_p^{shturb}	Ethanol	-7.13	351.44	398.23	456.69
β_p^{sh} , β_p^{shturb}	Benzene	-3.35	353.24	416.93	536.22
β_p^{sh} , β_p^{shturb}	Toluene	-4.88	383.73	448.92	553.66
β_p^{sh} , β_p^{shturb}	Tribrommethane	-2.95	422.35	456.84	505.54
κ_{sh_p} , $\kappa_{turbout_p}$	1,1,1,2-Tetrafluoroethane	-0.45	308.15	380.06	504.72
κ_{sh_p} , $\kappa_{turbout_p}$	1,1,1,3,3-Pentafluoropropane	-0.80	308.15	384.57	520.62
κ_{sh_p} , $\kappa_{turbout_p}$	Hexane	-1.32	341.88	436.72	561.34
κ_{sh_p} , $\kappa_{turbout_p}$	Ethanol	-1.01	351.44	411.37	504.48
κ_{sh_p} , $\kappa_{turbout_p}$	Benzene	-0.94	353.24	437.08	542.78

κ_{sh_p} , $\kappa_{turbout_p}$	Toluene	-1.25	383.73	433.00	540.77
κ_{sh_p} , $\kappa_{turbout_p}$	Tribrommethane	-0.88	422.35	486.66	579.96
$c_{p,\mathrm{vap}_p}^{wf}$, $\Delta H_{cond_p}^{wf}$	1,1,1,2-Tetrafluoroethane	1.7447e4	308.15	338.52	360.68
$c_{p,\mathrm{vap}_p}^{wf}$, $\Delta H_{cond_p}^{wf}$	1,1,1,3,3-Pentafluoropropane	2.5439e4	308.15	374.88	409.63
$c_{p,\mathrm{vap}_p}^{wf}$, $\Delta H_{cond_p}^{wf}$	Hexane	2.8801e4	341.88	429.07	484.80
$c_{p,\mathrm{vap}_p}^{wf}$, $\Delta H_{cond_p}^{wf}$	Ethanol	3.9185e4	351.44	445.68	503.59
$c_{p,\mathrm{vap}_p}^{wf}$, $\Delta H_{cond_p}^{wf}$	Benzene	2.8014e4	353.24	444.11	494.63
$c_{p,\mathrm{vap}_p}^{wf}$, $\Delta H_{cond_p}^{wf}$	Toluene	3.3280e4	383.73	504.55	573.08
$c_{p,\mathrm{vap}_p}^{wf}$, $\Delta H_{cond_p}^{wf}$	Tribrommethane	3.7524e4	422.35	589.62	662.01
c_{p,liq_p}^{wf}	1,1,1,2-Tetrafluoroethane	150.43	308.15	327.30	343.72
c_{p,liq_p}^{wf}	1,1,1,3,3-Pentafluoropropane	195.39	308.15	349.30	386.60
c_{p,liq_p}^{wf}	Hexane	213.00	341.88	402.74	464.26
c_{p,liq_p}^{wf}	Ethanol	138.31	351.45	420.01	472.08
c_{p,liq_p}^{wf}	Benzene	147.86	353.24	429.77	506.76
c_{p,liq_p}^{wf}	Toluene	184.06	383.76	483.04	537.85
c_{p,liq_p}^{wf}	Tribrommethane	160.30	422.35	517.44	597.88
$Z_{C_p}^{\left(1-\frac{T_{cond_j}^{wf}}{T_C}\right)^{2/7}}$	1,1,1,2-Tetrafluoroethane	0.44	308.15	328.29	344.44
$Z_{C_p}^{\left(1-\frac{T_{cond_j}^{wf}}{T_C}\right)^{2/7}}$	1,1,1,3,3-Pentafluoropropane	0.40	308.15	365.24	412.47
$Z_{C_p}^{\left(1-\frac{T_{cond_j}^{wf}}{T_C}\right)^{2/7}}$	Hexane	0.38	341.88	441.76	491.17
$Z_{C_p}^{\left(1-\frac{T_{cond_j}^{wf}}{T_C}\right)^{2/7}}$	Ethanol	0.36	351.45	447.69	498.54
$Z_{C_p}^{\left(1-\frac{T_{cond_j}^{wf}}{T_C}\right)^{2/7}}$	Benzene	0.37	353.24	486.14	542.57
$Z_{C_p}^{\left(1-\frac{T_{cond_j}^{wf}}{T_C}\right)^{2/7}}$	Toluene	0.37	383.76	510.44	566.877

$Z_{C_p}^{\left(1-\frac{T_{cond_j}^{wf}}{T_C}\right)^{2/7}}$	Tribrommethane	0.40	422.35	539.19	635.43

Table B.1 (Continued)

Property	*Working fluid*	A_4	α_1	α_2	α_3
Cp_p^{ig} (kJ/kmol/K)	1,1,1,2-Tetrafluoroethane	678.1	0.1701	0.1233	0.0891
Cp_p^{ig}	1,1,1,3,3-Pentafluoropropane	678.15	0.2361	0.1860	0.1275
Cp_p^{ig}	Hexane	678.15	0.3808	0.3082	0.2699
Cp_p^{ig}	Ethanol	678.15	0.1481	0.1264	0.1111
Cp_p^{ig}	Benzene	678.15	0.2828	0.2242	0.1753
Cp_p^{ig}	Toluene	678.15	0.3000	0.2705	0.2185
Cp_p^{ig}	Tribrommethane	678.15	0.0531	0.0435	0.0344
P_p^{sat} , P_p^{cond} (Pa)	1,1,1,2-Tetrafluoroethane	374.18	0.0293e6	0.0448e6	0.0655e6
P_p^{sat} , P_p^{cond}	1,1,1,3,3-Pentafluoropropane	427.2	0.0111e6	0.021366	0.04561e6
P_p^{sat} , P_p^{cond}	Hexane	507.6	0.0053e6	0.0138e6	0.0301e6
P_p^{sat} , P_p^{cond}	Ethanol	514	0.0100e6	0.0308e6	0.0685e6
P_p^{sat} , P_p^{cond}	Benzene	562.05	0.0072e6	0.0213e6	0.0435e6
P_p^{sat} , P_p^{cond}	Toluene	591.75	0.059e6	0.0169e6	0.035e6
P_p^{sat} , P_p^{cond}	Tribrommethane	678.15	0.0039e6	0.0148e6	0.0505e6
β_p^{sh} , β_p^{shturb}	1,1,1,2-Tetrafluoroethane	678.15	1.08e-2	4.13e-3	1.51e-3
β_p^{sh} , β_p^{shturb}	1,1,1,3,3-Pentafluoropropane	678.15	1.90e-2	7.39e-3	2.55e-3
β_p^{sh} , β_p^{shturb}	Hexane	678.15	2.65e-2	1.06e-2	4.39e-3
β_p^{sh} , β_p^{shturb}	Ethanol	678.15	8.71e-2	2.86e-2	4.83e-3
β_p^{sh} , β_p^{shturb}	Benzene	678.15	1.97e-2	7.79e-3	3.29e-3
β_p^{sh} , β_p^{shturb}	Toluene	678.15	2.90e-2	1.23e-2	5.47e-3
β_p^{sh} , β_p^{shturb}	Tribrommethane	678.15	2.17e-2	9.24e-3	3.92e-3
κ_{sh_p} , $\kappa_{turbout_p}$	1,1,1,2-Tetrafluoroethane	678.18	2.68e-3	1.08e-3	4.77e-4
κ_{sh_p} , $\kappa_{turbout_p}$	1,1,1,3,3-Pentafluoropropane	678.15	4.57e-3	1.82e-3	7.50e-4
κ_{sh_p} , $\kappa_{turbout_p}$	Hexane	678.15	6.50e-03	2.72e-03	1.29e-03
κ_{sh_p} , $\kappa_{turbout_p}$	Ethanol	678.15	9.43e-3	2.61e-3	6.67e-4

κ_{sh_p} , $\kappa_{turbout_p}$	Benzene	678.15	4.55e-3	2.06e-3	1.05e-3
κ_{sh_p} , $\kappa_{turbout_p}$	Toluene	678.15	1.37e-2	2.15e-3	4.88e-4
κ_{sh_p} , $\kappa_{turbout_p}$	Tribrommethane	678.15	3.35e-3	1.98E-3	1.35E-3
$c^{wf}_{p,\mathrm{vap}_p}, \Delta H^{wf}_{cond_p}$	1,1,1,2-Tetrafluoroethane	374.18	-122.2	-205.7	-679.8
$c^{wf}_{p,\mathrm{vap}_p}, \Delta H^{wf}_{cond_p}$	1,1,1,3,3-Pentafluoropropane	427.2	-108.5	-184.7	-670.4
$c^{wf}_{p,\mathrm{vap}_p}, \Delta H^{wf}_{cond_p}$	Hexane	507.6	-85.1	-152.1	-565.8
$c^{wf}_{p,\mathrm{vap}_p}, \Delta H^{wf}_{cond_p}$	Ethanol	514,0	-113.6	-276.3	-1198.9
$c^{wf}_{p,\mathrm{vap}_p}, \Delta H^{wf}_{cond_p}$	Benzene	507.6	-91.12	-182.90	-809.07
$c^{wf}_{p,\mathrm{vap}_p}, \Delta H^{wf}_{cond_p}$	Toluene	591.75	-76.36	-159.70	-702.26
$c^{wf}_{p,\mathrm{vap}_p}, \Delta H^{wf}_{cond_p}$	Tribrommethane	678.15	-80.52	-108.56	-476.50
c^{wf}_{p,liq_p}	1,1,1,2-Tetrafluoroethane	353.15	0.9914	1.024	1.675
c^{wf}_{p,liq_p}	1,1,1,3,3-Pentafluoropropane	427.2	0.3323	0.2609	0.2589
c^{wf}_{p,liq_p}	Hexane	507.6	0.4734	0.5743	0.6994
c^{wf}_{p,liq_p}	Ethanol	514	2.018	0.5742	0.4531
c^{wf}_{p,liq_p}	Benzene	562.05	0.3220	1.0046	0.3293
c^{wf}_{p,liq_p}	Toluene	591.75	0.4434	0.5659	0.6362
c^{wf}_{p,liq_p}	Tribrommethane	678.15	0.5576	0.8561	1.0665
$Z_{C_p}^{\left(1-\frac{T^{wf}_{cond_j}}{T_C}\right)^{2/7}}$	1,1,1,2-Tetrafluoroethane	353.75	1.88e-3	2.60e-3	3.88e-3
$Z_{C_p}^{\left(1-\frac{T^{wf}_{cond_j}}{T_C}\right)^{2/7}}$	1,1,1,3,3-Pentafluoropropane	427.2	1.19e-3	2.79e-3	2.73e-2
$Z_{C_p}^{\left(1-\frac{T^{wf}_{cond_j}}{T_C}\right)^{2/7}}$	Hexane	507.6	9.45e-4	2.54e-3	2.42e-2
$Z_{C_p}^{\left(1-\frac{T^{wf}_{cond_j}}{T_C}\right)^{2/7}}$	Ethanol	514.0	9.40e-4	2.83e-3	2.63e-2
$Z_{C_p}^{\left(1-\frac{T^{wf}_{cond_j}}{T_C}\right)^{2/7}}$	Benzene	562.0	7.98e-4	2.28e-3	2.03e-2
$Z_{C_p}^{\left(1-\frac{T^{wf}_{cond_j}}{T_C}\right)^{2/7}}$	Toluene	591.75	8.06e-4	1.93e-3	1.67e-2

$Z_{C_p}^{\left(1-\frac{T_{cond\,j}^{wf}}{T_C}\right)^{2/7}}$	Tribrommethane	678.15	4.82e-4	9.76e-4	2.51e-3

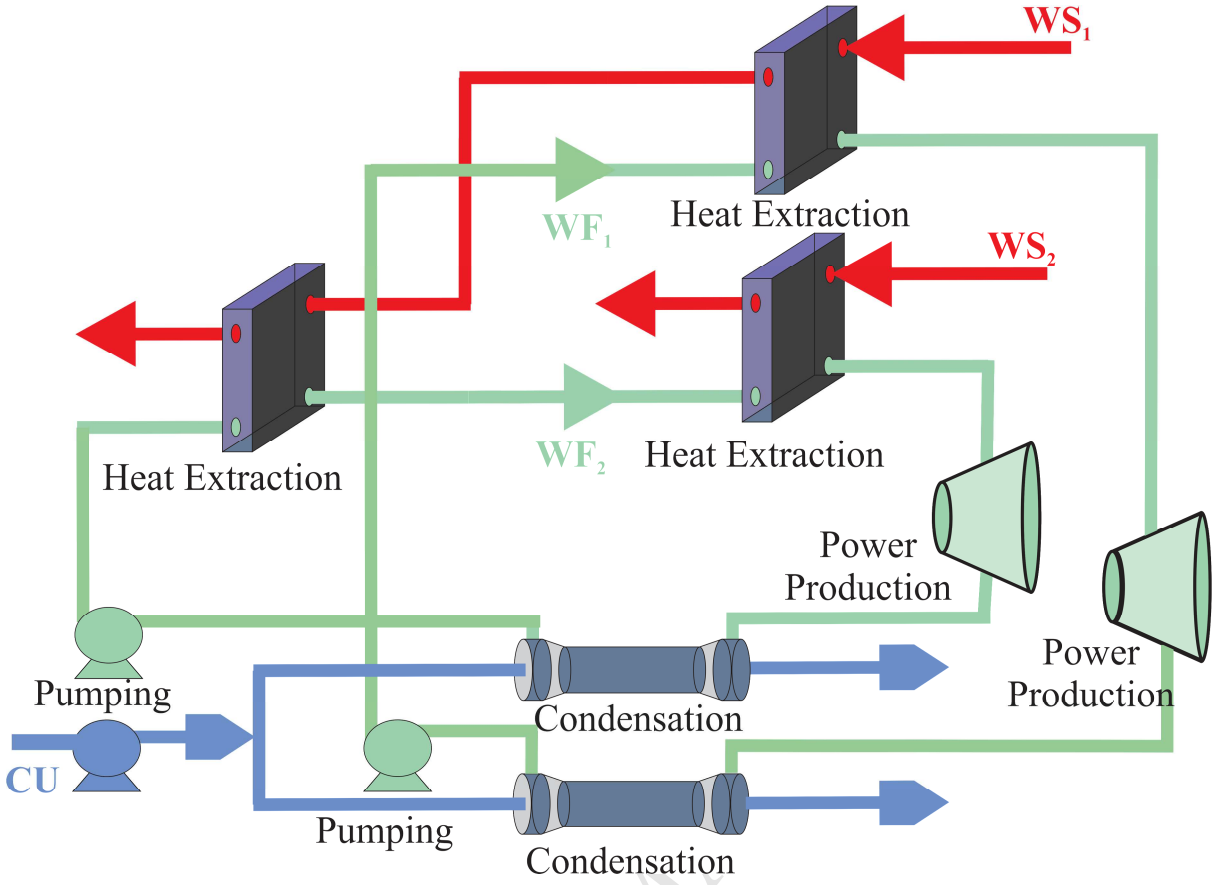

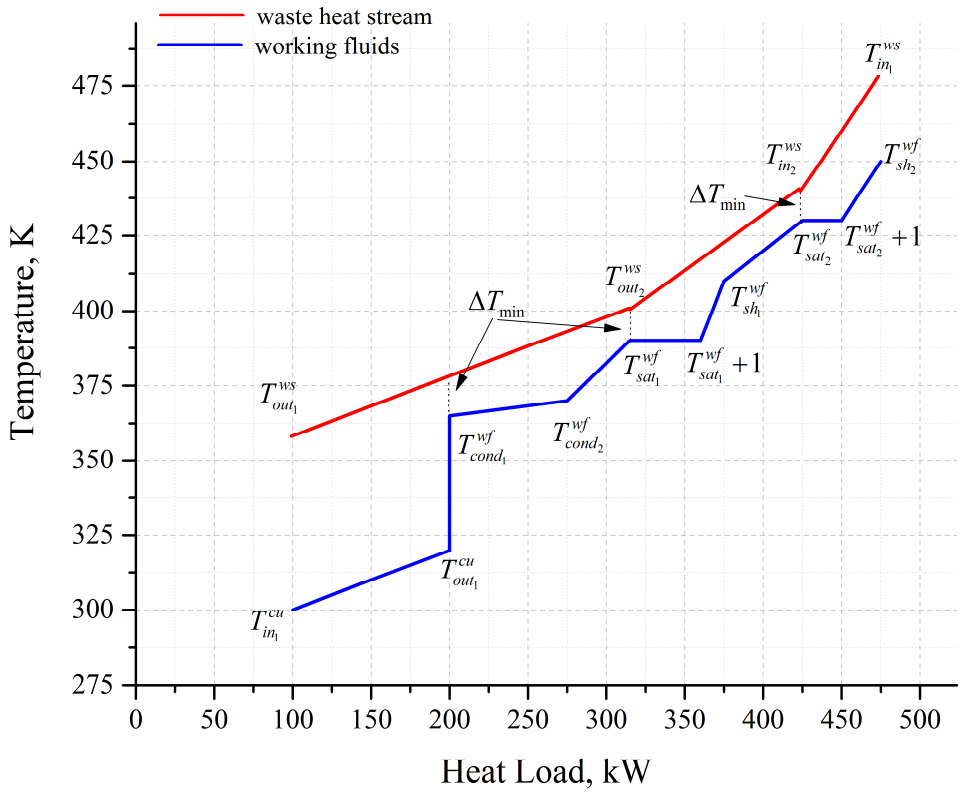

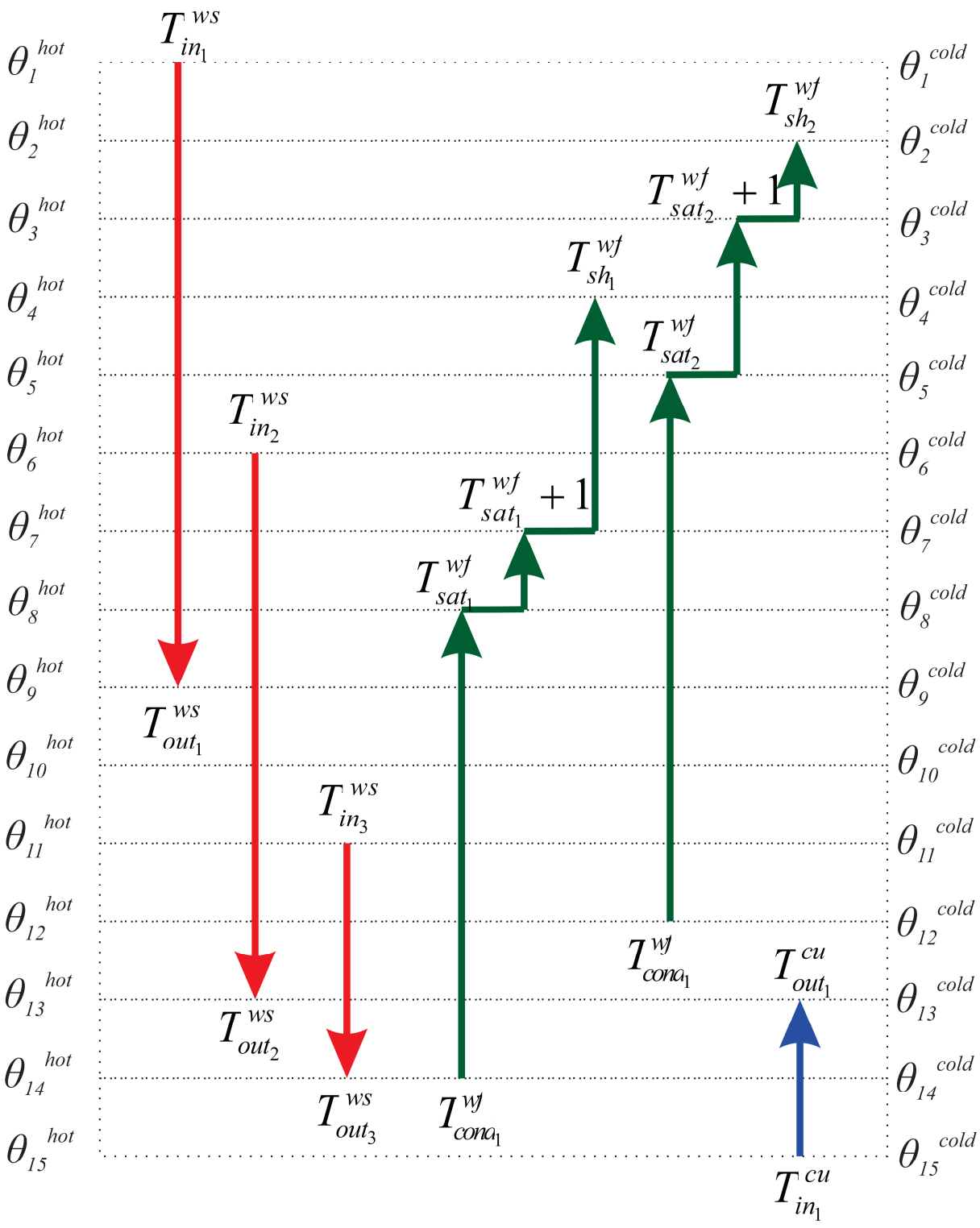
$T_{in_1}^{ws}$
$T_{in_2}^{ws}$
$T_{in_3}^{ws}$
$T_{out_1}^{ws}$
$T_{out_2}^{ws}$
$T_{out_3}^{ws}$
$T_{sat_1}^{wf}$
$T_{sat_1}^{wf}+1$
$T_{sh_1}^{wf}$
$T_{sat_2}^{wf}$
$T_{sat_2}^{wf}+1$
$T_{sh_2}^{wf}$
$T_{cona_1}^{wf}$
$T_{cona_1}^{wf}$
$T_{out_1}^{cu}$
$T_{in_1}^{cu}$
θ_1^{hot} θ_2^{hot} θ_3^{hot} θ_4^{hot} θ_5^{hot} θ_6^{hot} θ_7^{hot} θ_8^{hot} θ_9^{hot} θ_{10}^{hot} θ_{11}^{hot} θ_{12}^{hot} θ_{13}^{hot} θ_{14}^{hot} θ_{15}^{hot}
θ_1^{cold} θ_2^{cold} θ_3^{cold} θ_4^{cold} θ_5^{cold} θ_6^{cold} θ_7^{cold} θ_8^{cold} θ_9^{cold} θ_{10}^{cold} θ_{11}^{cold} θ_{12}^{cold} θ_{13}^{cold} θ_{14}^{cold} θ_{15}^{cold}

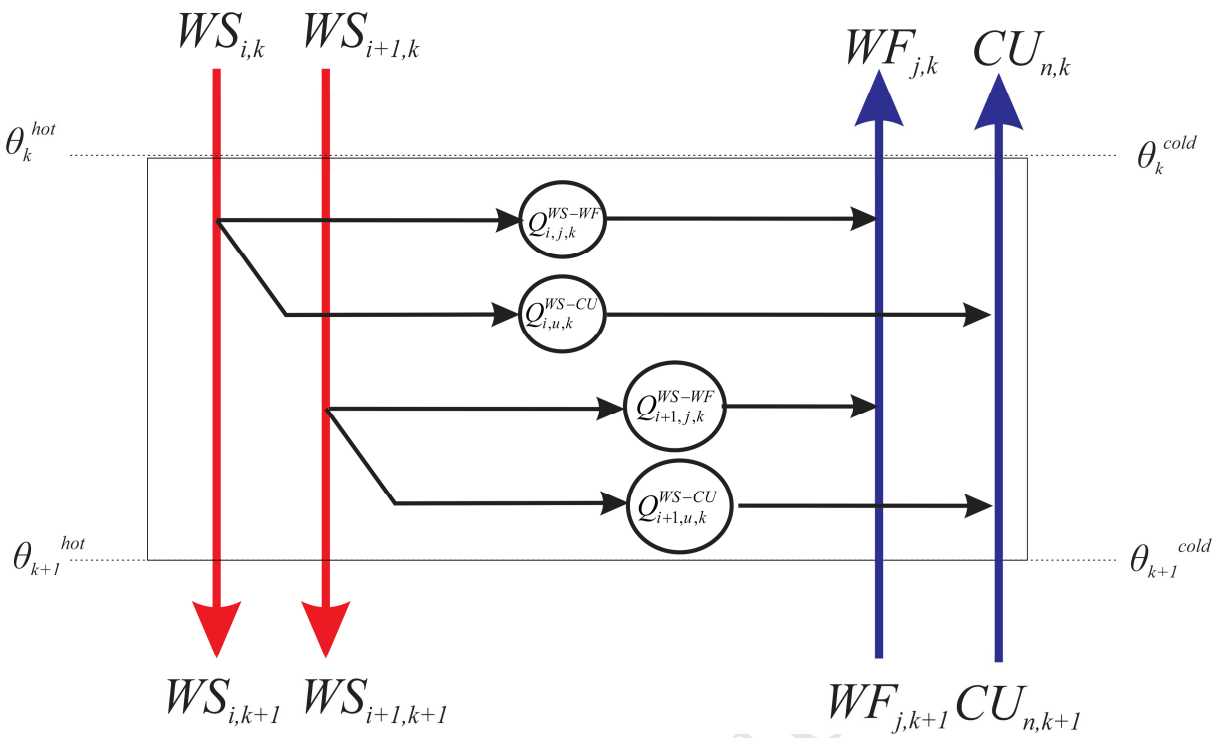

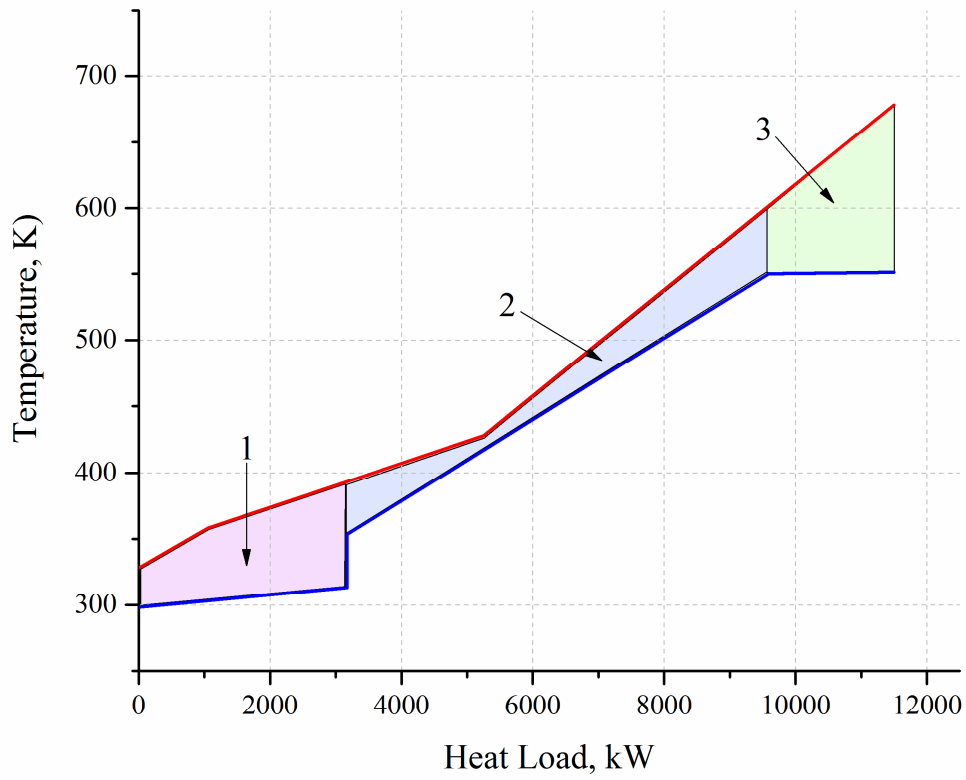

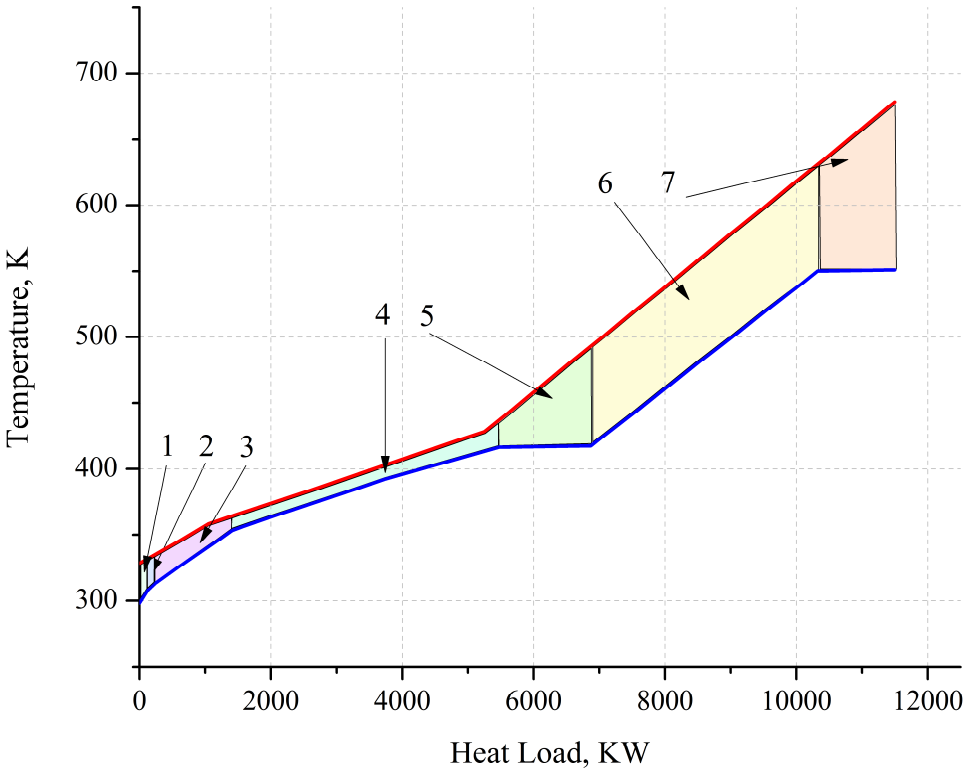

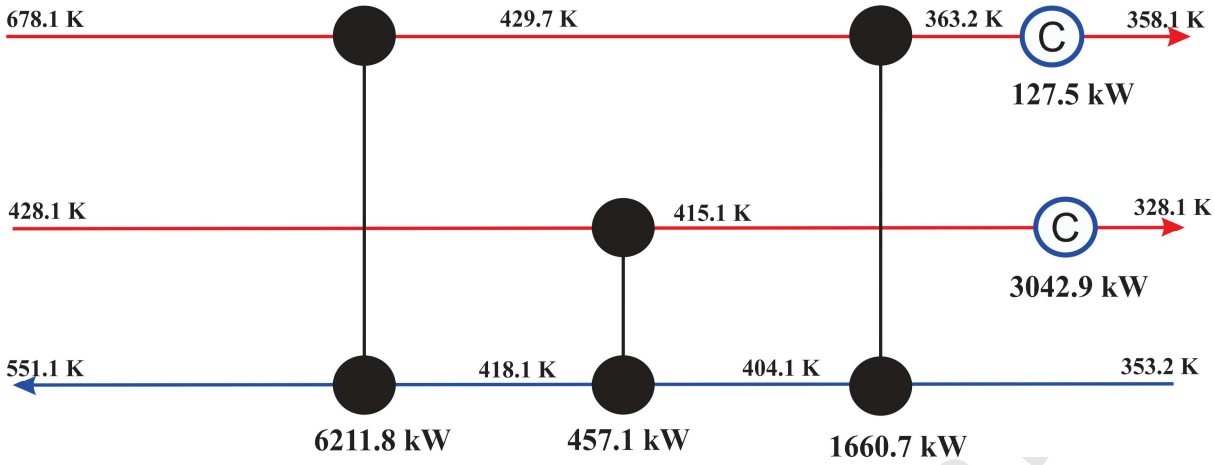

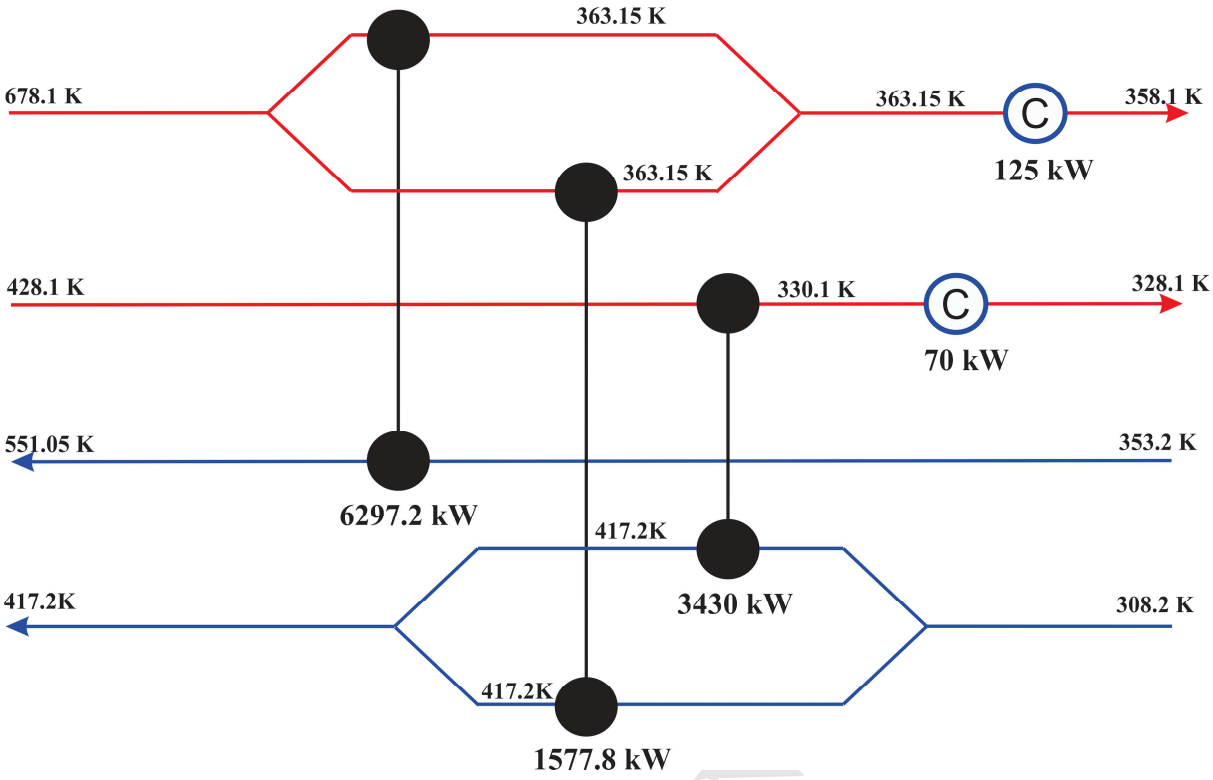

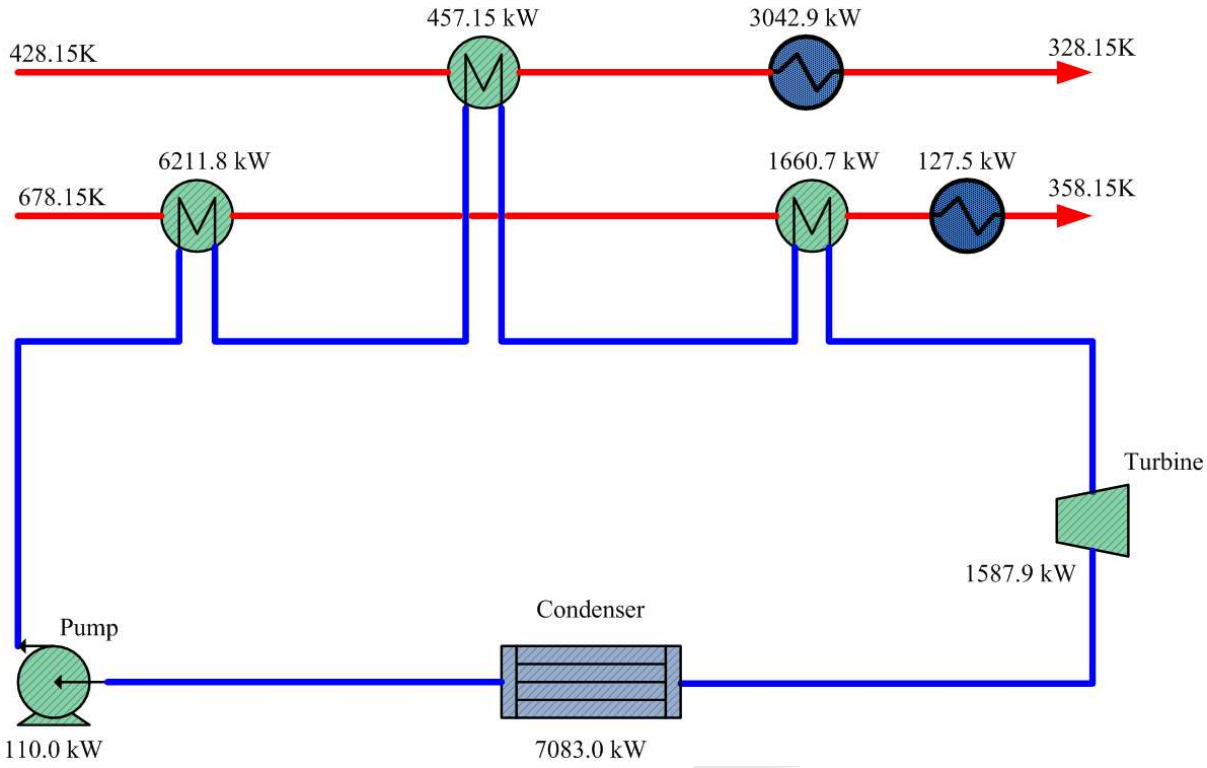

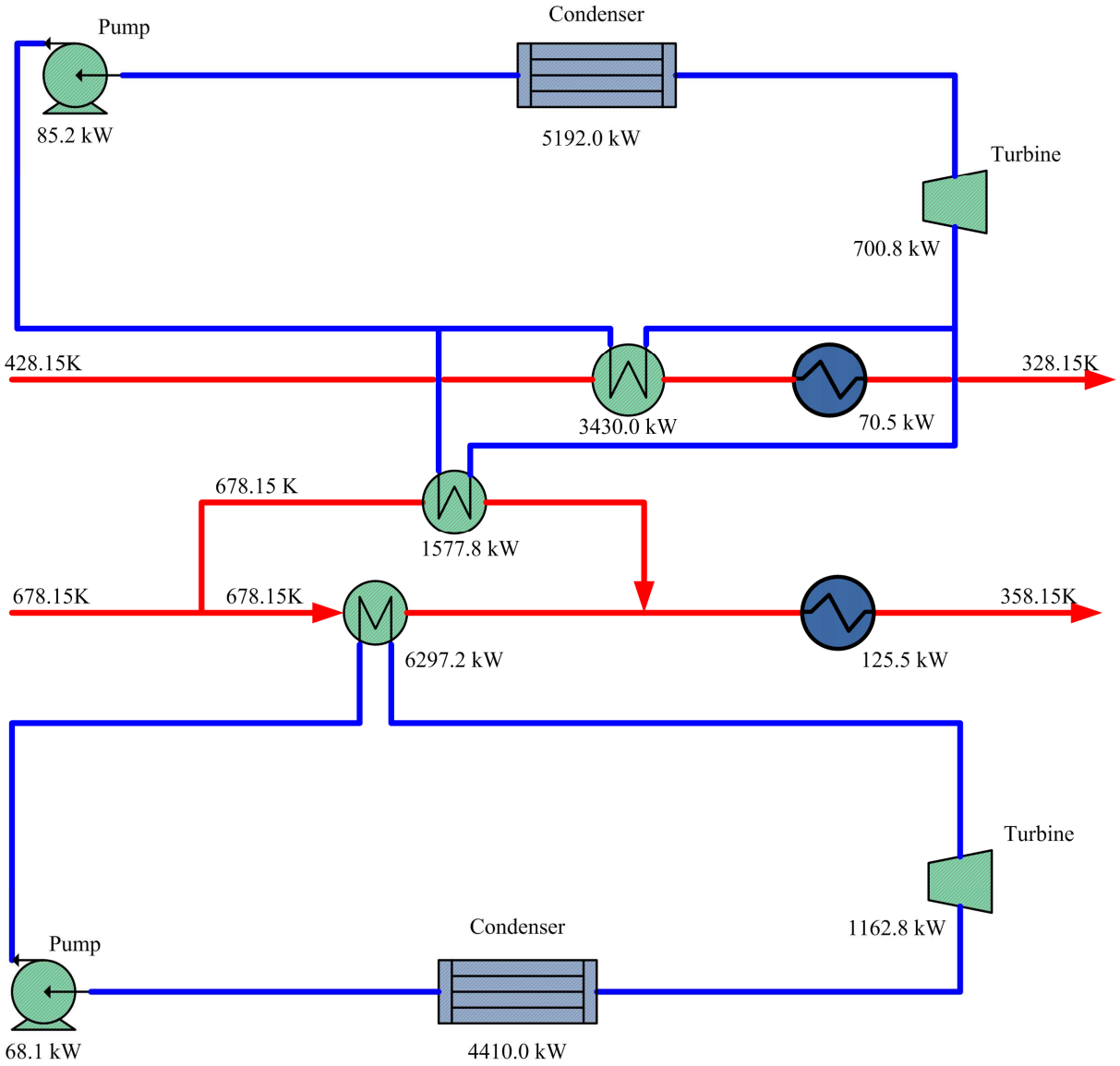

Highlights:

- Systematic approach to design an Organic Rankine Cycles
- Approach efficiently exploit more than one heat sources using multiple ORC cascades
- Approach includes the simultaneous selection of working fluids
- The design problem follows a mixed integer non-linear problem formulation
- An inclusive and flexible ORC model is automatically evolved